THE JOURNAL OF BIOLOGICAL CHEMISTRY VOL. 290, NO. 4, pp. 2379–2394, January 23, 2015

The C-terminal 50 Amino Acid Residues of Dengue NS3 Protein Are Important for NS3-NS5 Interaction and Viral Replication*

Received for publication, September 1, 2014, and in revised form, December 5, 2014 Published, JBC Papers in Press, December 8, 2014, DOI 10.1074/jbc.M114.607341

Moon Y. F. Tay[‡], Wuan Geok Saw[§], Yongqian Zhao[‡¶], Kitti W. K. Chan[‡], Daljit Singh[‡], Yuwen Chong[‡], Jade K. Forwood[‖], Eng Eong Ooi[‡], Gerhard Grüber[§], Julien Lescar[**], Dahai Luo[‡‡], and Subhash G. Vasudevan[‡¶1]

*From the [‡]Program in Emerging Infectious Diseases, Duke-National University of Singapore Graduate Medical School, 8 College Road, Singapore 169857, Singapore, the [§]School of Biological Sciences, Nanyang Technological University, 60 Nanyang Drive, Singapore 637551, Singapore, the [¶]NUS Graduate School for Integrative Sciences and Engineering, National University of Singapore, 28 Medical Drive, Singapore 117456, Singapore, the [‖]School of Biomedical Sciences, Charles Sturt University, Wagga Wagga, New South Wales 2650, Australia, the **Division of Structural Biology and Biochemistry, School of Biological Sciences, Nanyang Technological University, Singapore 138673, Singapore, and the [‡‡]Lee Kong Chian School of Medicine, Nanyang Technological University, 61 Biopolis Drive, Proteos Building, 07-03, Singapore 138673, Singapore*

Background: NS3-NS5 interaction is important for the dengue virus life cycle.
Results: NS3 residue Asn-570 is essential for its interaction with NS5; mutation in an infectious cDNA abolished virus production and reduced positive-strand RNA synthesis.
Conclusion: NS3-NS5 interaction may be required for coordinated positive- and negative-strand RNA synthesis.
Significance: NS3-NS5 interaction may be a target for rational design of antiviral drugs.

Dengue virus multifunctional proteins NS3 protease/helicase and NS5 methyltransferase/RNA-dependent RNA polymerase form part of the viral replication complex and are involved in viral RNA genome synthesis, methylation of the 5′-cap of viral genome, and polyprotein processing among other activities. Previous studies have shown that NS5 residue Lys-330 is required for interaction between NS3 and NS5. Here, we show by competitive NS3-NS5 interaction ELISA that the NS3 peptide spanning residues 566–585 disrupts NS3-NS5 interaction but not the null-peptide bearing the N570A mutation. Small angle x-ray scattering study on NS3(172–618) helicase and covalently linked NS3(172–618)-NS5(320–341) reveals a rigid and compact formation of the latter, indicating that peptide NS5(320–341) engages in specific and discrete interaction with NS3. Significantly, NS3:Asn-570 to alanine mutation introduced into an infectious DENV2 cDNA clone did not yield detectable virus by plaque assay even though intracellular double-stranded RNA was detected by immunofluorescence. Detection of increased negative-strand RNA synthesis by real time RT-PCR for the NS3:N570A mutant suggests that NS3-NS5 interaction plays an important role in the balanced synthesis of positive- and negative-strand RNA for robust viral replication. Dengue virus infection has become a global concern, and the lack of safe vaccines or antiviral treatments urgently needs to be addressed. NS3 and NS5 are highly conserved among the four serotypes, and the protein sequence around the pinpointed amino acids from the NS3 and NS5 regions are also conserved. The identification of the functionally essential interaction between the two proteins by biochemical and reverse genetics methods paves the way for rational drug design efforts to inhibit viral RNA synthesis.

Dengue virus (DENV),[2] of which there are four distinct serotypes (DENV1–4), is an important re-emerging mosquito-borne flavivirus that is endemic in more than 100 countries, causing >390 million human infections that result in ~100 million dengue fever (DF) cases (1). Infections with DENV are either asymptomatic or can result in self-limiting febrile illness (DF) that leads to a broad spectrum of pathologies, including severe DF without hemorrhagic symptoms, dengue hemorrhagic fever, or dengue shock syndrome. The current treatment for dengue infection is mainly supportive, and there is no preventative vaccine or effective antiviral agents to treat DF or the more severe disease manifestations.

The ~11-kb positive-sense single-stranded RNA genome of DENV serotypes share around 70% sequence identity and contain a 5′-type-1 cap as well as 5′- and 3′-untranslated regions (UTR) that flank a single open reading frame (ORF) (2). An ~3300-amino acid polyprotein precursor is translated from the ORF and is processed by both host and viral proteases to yield three structural proteins (capsid, premembrane protein, and envelope protein (E)) and seven nonstructural proteins (NS) (NS1, NS2A, NS2B, NS3, NS4A, NS4B, and NS5) that are

* This work was supported by the Duke-National University of Singapore Signature Research Program (funded by the Ministry of Health, Singapore), National Medical Research Council, Singapore, Grants NMRC/1315/2011 and NMRC/TCR/005/2008, and the Ministry of Education MOE Tier 3 Grant MOE2012-T3-1-008, Singapore.
[1] To whom correspondence should be addressed. Tel.: 65-6516-6718; Fax: 65-6221-2529; E-mail: subhash.vasudevan@duke-nus.edu.sg.

[2] The abbreviations used are: DENV, Dengue virus; SAXS, small-angle x-ray scattering; RdRP, RNA-dependent RNA polymerase; P/S, penicillin/streptomycin; bNLS, importin b-mediated nuclear localization sequence; NSD, normalized spatial discrepancy; NSD, normalized spatial discrepancy; IFA, immunofluorescence assay; EOM, ensemble optimization method; E, envelope protein; DF, dengue fever; RC, replication complex; Y2H, yeast two-hybrid.

TABLE 1
List of proteins/peptides used in ELISA, SAXS and viral inhibition assay

Protein/peptide name	Vector	Tag	Residue number	Ref.
His-NS5 RdRP	pET15b (Novagen)	His_6 (not removed)	273–900 of DENV3 NS5	Yap *et al.* (25)
$NS2B_{18}NS3$	pET32b (Novagen)	Thioredoxin (removed)	49–66 of DENV3 NS2B and 1–618 of DENV3 NS3 connected by G_4SG_4 linker	Luo *et al.* (11)
His-NS3(172–618)	pET14b (Novagen)	His_6 (not removed)	172–618 of DENV3 NS3	In this study
GST-NS3(482–618)	pGEX-4T-1 (GE Healthcare)	Glutathione *S*-transferase (GST; not removed)	482–618 of DENV3 NS3	
GST-NS3(566–618)		GST (not removed)	566–618 of DENV3 NS3	
NS3(172–618)	pET32b (Novagen)	His_6 (removed)	172–618 of DENV4 NS3	Luo *et al.* (11)
NS3(172–618)-G_4SG_4-NS5(320–341)	pProEx HTb (Invitrogen)		172–618 of DENV4 NS3 and 320–341 of DENV4 NS5 connected by G_4SG_4 linker	In this study
NS3(566–585)	Synthesized by NTU peptide synthesis		566–585 of DENV3 NS3	In this study
NS3(566–585) (N570A)	core facility (Singapore)		566–585 of DENV3 NS3, with N570A	
NS3(570–585)			570–585 of DENV3 NS3	
NS3(86–100)			86–100 of DENV3 NS3	
Penetratin (p)		Biotin	Third α-helix of the Antennapedia homeodomain (56)	
$_pNS5(320–341)$			320–341 of DENV3 NS5 connected to penetratin sequence	
$_pNS5(s320–341)$			Scrambled sequence of 320–341 of DENV3 NS5 connected to penetratin sequence	

involved in formation of mature virion and viral RNA replication, respectively. Among the NS proteins, NS3 and NS5 contain the enzymatic activities that are essential for DENV replication (3).

Both NS3 (residues 1–618) and NS5 (residues 1–900) are large multifunctional proteins with sequence identity of around 60 and 70% among the four serotypes, respectively (3). NS3 contains an N-terminal serine protease domain (residues 1–170) that requires NS2B to be an active protease (4–8). Its C-terminal domain contains ATPase/helicase activity for unwinding of the double-stranded RNA (dsRNA) intermediate (9–14) and RNA 5′-triphosphatase activity for viral RNA 5′-capping reaction that is carried out together with the N-terminal domain of NS5, which has methyltransferase activity (3, 9, 13, 15–22). The C-terminal domain of NS5 has RNA-dependent RNA polymerase (RdRP) activity, which is crucial for RNA replication (19, 23–26). NS3 and NS5 have been shown to interact and colocalize in infected cells, and NS3 RNA 5′-triphosphatase activity has been reported to be stimulated by NS5 *in vitro* (9, 27–29). These observations are consistent with the functional roles of both NS3 and NS5 in the replication complex (RC) (30, 31).

During viral RNA replication within the RC, many critical RNA-RNA, RNA-protein, and protein-protein interactions occur to synthesize both positive- and negative-strand viral RNA (31, 32). There have been several reports of NS3-NS5 interactions that include biochemical pulldown assays from infected cell extracts (28, 32–34) and two-hybrid (Y2H) studies that mapped the interaction to the C-terminal region of NS3 helicase (residues 303–618) and the N-terminal region of NS5 RdRP (residues 320–368; known as bNLS (nuclear localization sequence)) (35, 36). The NS5-binding site appears to be centered at residue Lys-330 because the mutation to alanine disrupted its interaction with NS3 and abolished RNA replication, although the *in vitro* RdRP activity was unaffected (37). Based on available crystal structures of the RdRP domain of NS5, it has been proposed that the cavity occupied by Lys-330 may be a potential target for antiviral drug design by blocking NS3-NS5 interaction (37). However, the details of the interaction from the NS3 perspective is missing to fully exploit structure-guided drug design.

In this study, through the use of both NS3 WT and mutant peptides in competitive NS3-NS5 interaction ELISA, we identified a conserved amino acid in subdomain III of DENV NS3 protein, Asn-570, as being critical for its interaction with NS5. Mutation of NS3:Asn-570 to alanine in the DENV2 cDNA clone abolished infectious virus production and reduced viral protein production and RNA replication. This mutation also suggests that the NS3-NS5 interaction is essential for viral RNA replication by possibly coordinating positive- and negative-strand synthesis. Small angle x-ray scattering (SAXS) data of NS3 helicase (residues 172–618) covalently linked to NS5(320–341) supports the observation that physical interaction occurs in the region of interaction between NS3 and NS5.

EXPERIMENTAL PROCEDURES

Cell Lines and Virus—Baby hamster kidney cells (BHK-21) were cultured in RPMI 1640 medium (Invitrogen) supplemented with 10% fetal bovine serum (FBS), 100 units/ml penicillin, and 100 μg/ml streptomycin (1% P/S) in 5% CO_2 at 37 °C.

Human hepatoma (Huh-7) cells were cultured in DMEM (Invitrogen) supplemented with 10% FBS and 1% P/S at 37 °C, with 5% CO_2. *Aedes albopictus* mosquito (C3/36) cells were cultured in RPMI 1640 medium supplemented with 25 mM HEPES, 10% FBS, and 1% P/S at 28 °C, in the absence of CO_2.

DENV2 of cosmopolitan genotype (GenBank™ number EU081177.1) that was used in this study was grown in C3/36 cells and titered in BHK-21 cells before storage at −80 °C. This virus was isolated during a local dengue outbreak that occurred in 2005 as part of Early Dengue Infection and Outcome (EDEN) Study in Singapore (38).

Plasmid Construction—Plasmids for the expression of DENV3 NS5 RdRP (residues 273–900), NS3 full-length protein ($NS2B_{18}NS3$; residues 49–66 of NS2B and 1–618 of NS3 connected by a flexible linker G_4SG_4), and DENV4 NS3 helicase domain (NS3(172–618)) have been described previously (Fig. 1*A* and Table 1) (11, 25, 39).

DENV3 NS3(172–618), NS3(482–618), and NS3(566–618) fragments were amplified from DENV3 NS2B$_{18}$NS3 construct (as mentioned above). NS3(172–618) fragment was amplified with forward primer 5′-CAAACAAATGCACATATGGATG-GACCGACACC-3′ and the reverse primer 5′-GTGCTCGAG-TGCGGATCCAAGCTTTTACTTTC-3. The underlined sequence corresponds to NdeI and BamHI sites, respectively. The PCR fragment was digested with NdeI and BamHI and cloned into pET14b (Novagen, Germany). The NS3(482–618) fragment was amplified with the forward primer 5′-CCAGCCTCTCGGATCCGATGAAGACCATG-3′ and the reverse primer 5′-CACAAGATCAAGCTCGAGTCACTTTCTGCC-3′. The NS3(566–618) fragment was amplified with the forward primer 5′-GAAAATGGTGCGGATCCGGGCAACGCAATAATC-3′ and the same reverse primer as above. The underlined sequence corresponds to BamHI and XhoI sites, respectively. Both PCR products were digested with BamHI and XhoI and cloned into pGEX-4T-1 (GE Healthcare) (Fig. 1*A* and Table 1).

DENV4 NS3(172–618)-NS5(320–341) fragment (connected by a flexible linker G_4SG_4, Fig. 3*A* and Table 1) was amplified from DENV4 NS2B$_{18}$NS3 construct (as mentioned above). The full-length PCR product was generated by first amplifying the helicase region with the forward primer 5′-GAAAAC-CTGTATTTTCAGGGCGCCGGCGGTGAGCCAGATTAT-GAAGTGG-3′ and the reverse primer 5′-CTCCATTCACCA-TTCCTCCTCCTCCTGATCCTCCTCCTCCCTTTCTTCC-ACTGGC-3′, followed by two separate PCRs that added the flexible linker sequence and NS5(320–341) sequence to the helicase via two reverse primers, 5′-GGAATCACAT-CCCAGGGTTTTGTCAGCAGTTTCACCACTCCATTCA-CCATTCCTC-3′ and 5′-GCGGCCGCGACTAGTGAGCTC-GTCGACTTACTGGGTCACCATTGGAATCACATCCCA-GGG-3′. The underlined sequence corresponds to NaeI and SalI sites, respectively. The PCR product was digested with NaeI and SalI and cloned into pProEx HTb vector.

Mutation of NS3 Asn-570 to alanine in DENV3 NS2B$_{18}$NS3 was done using QuikChange II XL site-directed mutagenesis kit (Stratagene), according to the manufacturer's protocol. The following primers were used: NS3 N570A forward (5′-GATGGGC-AACGCAATGCTCAAATTTTAGAGGAG-3′) and reverse (5′-CTCCTCTAAAATTTGAGCATTGCGTTGCCCATC-3′). The underlined nucleotide corresponds to the mutation that was being made. Mutations were confirmed by automated DNA sequencing.

Protein Expression and Purification—For ELISA and ATPase activity assay, NS3 and NS5 constructs (Table 1) were transformed into *Escherichia coli* BL21 CodonPlus (DE3)-RIL cells (Stratagene) for protein expression and purified as previously published (11, 25, 39).

For SAXS, NS3(172–618) and NS3(172–618)-NS5(320–341) constructs were transformed into *E. coli* BL21 CodonPlus (DE3)-RIL cells (Stratagene) for protein expression and purified as described below. The cells were disrupted on ice by sonication three times for 1 min in buffer A (20 mM sodium phosphate, pH 7.4, 500 mM NaCl, 0.8 mM DTT, and 2 mM Pefabloc^{SC} (Biomol)). Precipitated material was separated by centrifugation at 12,500 × *g* for 25 min, and the supernatant was filtered (0.45 μm; Millipore). The filtered supernatant was incubated with 2 ml of nickel-nitrilotriacetic acid-agarose (Qiagen) for 1.5 h at 4 °C, and the His$_6$-tagged protein was eluted with an imidazole gradient from 20 to 200 mM in buffer A. Fractions containing the protein of interest were pooled and subjected to overnight cleavage with thrombin for NS3(172–618) or tobacco etch virus protease for NS3(172–618)-NS5(320–341) and dialyzed overnight in buffer B (20 mM sodium phosphate, pH 7.4, 200 mM NaCl) at 4 °C. Following incubation, the dialyzed sample was incubated with 1 ml of nickel-nitrilotriacetic acid-agarose for 1 h at 4 °C, and the flow-through containing cleaved NS3(172–618) or NS3(172–618)-NS5(320–341) was collected and applied to a gel filtration column (Superdex^{TM} 200 HR 10/300 column, GE Healthcare) in buffer C (20 mM Tris/HCl, pH 7.4, 200 mM NaCl, 5% glycerol, 1 mM DTT). Fractions containing NS3(172–618) or NS3(172–618)-NS5(320–341) were pooled and concentrated using Amicon Ultra-4 centrifugal unit (10-kDa molecular mass cutoff; Millipore).

Peptide Synthesis—Peptides were synthesized at the Nanyang Technological University peptide synthesis core facility (Singapore).

Competitive NS3-NS5 Interaction ELISA—The ELISA (Fig. 1*B*) was performed as published previously (33). The concentration of NS2B$_{18}$NS3 was fixed at 60 or 80 nM and mixed with increasing concentrations of truncated NS3 proteins (DENV3 NS3(172–618), GST-NS3(482–618), GST-NS3(566–618), or GST (negative control)) or NS3 peptides (NS3(566–585) and NS(566–585) (N570A), NS(571–585), or NS(86–100) (negative control); listed in Table 1). The concentration of NS3 protein at which 50% inhibition of NS2B$_{18}$NS3 protein binding occurs represents the apparent K_D value for the DENV3 NS5 RdRP-NS3 protein interaction. Data were fitted to the sigmoidal dose-response equation (variable slope) by nonlinear regression using GraphPad Prism 5 from triplicate measurements.

Viral Inhibition Assay—2×10^5 Huh-7 cells were seeded into a 12-well plate and incubated overnight at 37 °C with 5% CO_2. Cells were infected with DENV2 at a multiplicity of infection of 1 for 1 h, after which the virus inocula were then removed and replaced with 5% FBS/DMEM maintenance media. At 6 h post-infection, the infected cells were treated with 7.5 μM NS3 peptides complexed with 22.5 μM penetratin in a molar ratio of 1:3 or 7.5 μM NS5-penetratin fusion peptides (Table 1). At 24 h post-infection, cells were washed once with PBS prior to lysis by TRIzol for cellular viral RNA quantification by real time RT-PCR analysis with primers that binds to the NS1 gene (forward 5′-CCGCTGACATGAGTTTTGAGTC-3′ and reverse 5′-CATGACAGGAGACATCAAAGGA-3′) (40).

ATPase Activity Assay—The assay was carried out as described (13), with slight modifications. Purified NS2B(320–368)NS3 WT or N570A protein of 2.5 nM was preincubated at 37 °C with poly(U) (10 μg/ml) in 40 μl of reaction buffer (50 mM Tris/HCl, pH 7.5, 2 mM $MgCl_2$, 1.5 mM dithiothreitol, 0.05% Tween 20, 0.25 μg/ml bovine serum albumin (Sigma)) for 5 min. The reaction was initiated by the addition of 10 μl of varying ATP concentrations (2-fold serial dilution, starting from 2000 μM) and carried out for 10 min at 37 °C. 10 μl of malachite green reagent (BioAssay Systems) was added to stop the reaction. Absorbance was read at 635 nm after 30 min at room temperature. The K_m of the protein was determined with GraphPad Prism 5, with Michaelis-Menten Equation 1,

$$V_o = (V_{max}[S])/(K_m + [S]) \quad \text{(Eq. 1)}$$

SAXS—SAXS data of the NS3(172–618) and NS3(172–618)-NS5(320–341) were measured by the NanoStar™ instrument (Bruker), equipped with a METALJET™ x-ray source and Vantec 2000-detector system. The METALJET™ source uses the liquid gallium source to deliver a high intensity x-ray beam at the wavelength of $\lambda = 1.34$ Å. The SAXS measurements were carried out with the source to sample distance of 145 cm, a two-pinhole collimation system, and the sample to detector distance of 67 cm (41). SAXS experiments of both proteins were carried out at 1.2, 2.2, and 4 mg/ml in a sample volume of 40 μl at 15 °C. For each sample, a total of nine measurements at 5-min intervals were recorded. The data were flood-field and spatially corrected, and processed using the built-in SAXS software. We tested the possible radiation damage by comparing all data sets, and no changes were detected. The scattering intensity of the buffer was subtracted, and the difference curves were scaled for the concentration. All the data processing steps were performed automatically using the program package PRIMUS (42). The forward scattering $I(0)$ and the radius of gyration R_g were evaluated using the Guinier approximation (43). These parameters were also computed from the entire scattering patterns using the indirect transform package GNOM (44), which also provides the distance distribution function $p(r)$. Ten low resolution models of NS3(172–618) or NS3(172–618)-NS5(320–341) were independently built by the program GASBOR (45). The spatial discrepancy (NSD), which is a measure of similarity between sets of three-dimensional points, was computed between all 10 reconstructions using the DAMAVER program (46). The reconstruction with the least NSD was selected for NS3(172–618) or the fusion protein NS3(172–618)-NS5(320–341). The ensemble optimization method (EOM) suite was used to select an ensemble of conformations that best fit the experimental data, and the dimensions of selected conformations were compared with the random pool to evaluate the flexibility and compactness of NS3(172–618)-NS5(320–341) (47, 48).

DENV2 Full-length cDNA Clone Construction and Site-directed Mutagenesis—To construct a full-length DENV2 cDNA clone (GenBank™ accession EU081177.1, cosmopolitan genotype; Fig. 4*A*), low passage virus stock was subjected to viral RNA extraction by RNeasy kit (Qiagen), and three cDNA fragments (fragment boundaries indicated by nucleotide numbers; Fig. 4*A*) covering the complete genome were amplified from viral RNA by RT-PCR using SuperScript III one-step RT-PCR kits (Invitrogen). Fragment 1 contained the SphI restriction site, a T7 promoter sequence, and DENV2 cDNA nucleotides 1–4498, which also contained the KpnI restriction site. Fragment 2 spanned from the KpnI site (nucleotide position 4493) to the XbaI site (nucleotide position 6008). Fragment 3 spanned from XbaI site (nucleotide position 6003) to the 3′ end of the genome (nucleotide position 10,723), containing the SacI site at the end of the genome. The PCR product of each cDNA fragment was digested and cloned into a pre-digested and modified low copy number plasmid pWSK29 (49). The plasmid was modified by the replacement of the BssHII site that was located before the T7 promoter with the SphI site by site-directed mutagenesis of the plasmid with the following primer: forward 5′-GGCCAGTGAGCATGCGTAATACGAC-3′ and reverse 5′-GTCGTATTACGCATGCTCACTGGCC-3′. The underlined nucleotide corresponds to the mutation that was being made. The subclone that maintained each fragment was named accordingly as follows: pWSK29 D2 fragment 1, fragment 2, and fragment 3, respectively, and each subclone was validated by DNA sequencing by 1st BASE DNA Sequencing Services (Singapore) before proceeding for assembly. Subsequently, fragment 2 was inserted into the subclone pWSK29 D2 fragment 1 at the KpnI and XbaI site to generate subclone pWSK29 D2 fragment 1 + 2. Finally, fragment 3 was inserted to generate subclone pWSK29 D2 fragment 1 + 2 at XbaI and SacI sites to generate the full-length cDNA clone, pWSK29 D2 full length. The *E. coli* XL-1 Blue chemically competent cell (Stratagene) was used for construction and propagation of the cDNA clones. Standard cloning procedures were performed with the exception that the cDNA clones were propagated at 30 °C for at least 20 h. All restriction enzymes were purchased from New England Biolabs.

The genome-length cDNA clones with NS3:N570A and NS5:K330A mutations were constructed using the subclone pWSK29 D2 fragment 3. The mutations were generated using QuikChange II XL site-directed mutagenesis kit (Stratagene) and performed according to the manufacturer's protocol. The following primers were used for the generation of both mutants: NS3:N570A forward (5′-CTTTGATGGAGTCAAGAACGCCCAAATCTTGGAAGAAAATG-3′) and reverse (5′-CATTTTCTTCCAAGATTTGGGCGTTCTTGACTCCATCAAAG-3′); NS5:K330A forward (5′-GTGGTTAGGCTGCTAACAGCACCTTGGGATGTCATCCCC-3′) and reverse (5′-GGGGATGACATCCCAAGGTGCTGTTAGCAGCCTAACCAC-3′). The underlined nucleotides correspond to the mutation that was being made. Mutations were confirmed by automated DNA sequencing, and fragment 3 bearing the mutation was excised from the plasmid by XbaI and SacI and inserted into subclone pWSK29 D2 fragments 1 + 2 that were similarly cut with XbaI and SacI.

In Vitro Transcription, RNA Electroporation, Plaque Assay, Real Time RT-PCR (Reverse Transcription-PCR), Immunofluorescence Assay (IFA), and Western Blot—BHK-21 cells were trypsinized, washed twice with cold PBS, and resuspended in Opti-MEM (Invitrogen) at a cell density of 1×10^7 cells/ml. 10 μg of *in vitro* transcribed RNA with T7 mMESSAGE mMACHINE kit (Ambion) of DENV2 WT and mutants were mixed with 800 μl of cell suspension in a pre-chilled 0.4-cm cuvette and electroporated at settings of 850 V and 25 microfarads, 2 pulses with an interval of 3 s. Electroporated cells were allowed to recover at room temperature for 10 min before resuspending in complete RPMI 1640 medium for cell recovery. Cells (3×10^5) were then seeded into a 12-well plate and incubated at 37 °C in the presence of 5% CO_2. Media were changed to 2% FBS maintenance media after 6 h post-transfection. Samples were harvested every 24 h post-transfection until 120 h. Supernatants were collected and clarified for titering of the infectious virus particle by standard plaque assay and extracellular viral RNA quantification by real time RT-PCR analysis (40). Cells were then washed once with PBS prior to lysis by TRIzol reagent (Invitrogen) or 1× SDS-

PAGE reducing loading dye for cellular viral RNA quantification and Western blot, respectively.

For cellular viral RNA quantification, total RNA was isolated using the TRIzol extraction method from the cell lysate. 500 ng of total RNA was used for cDNA synthesis using the Improm II reverse transcription system (Promega) with random primer in accordance to manufacturer's instructions. 40 ng of cDNA was used for real time RT-PCR analysis of viral RNA in Bio-Rad iQ-5 real time thermal cycler with the use of SYBR Green supermix (Bio-Rad) as described previously with primers that bind to the NS1 gene (forward 5′-CCGCTGACATGAGTTTTGAGTC-3′ and reverse 5′-CATGACAGGAGACATCAAAGGA-3′) (40). Absolute numbers of intracellular viral RNA genome copy were quantitated using the DENV standard curve, normalized to actin levels, and reported as absolute number of viral RNA genome copy per μg of RNA used for real time RT-PCR.

For intracellular viral RNA genome copy of both positive and negative strands, 5′-tagged primers that bind to the E gene (Eden2_forward_RT, 5′-GGCCGTCATGGTGGCGAATAACAGGCTATGGCACTGTCACGAT-3′, and Eden2_reverse_RT, 5′-GGCCGTCATGGTGGCGAATAACCATTTGCAGCAACACCATCTC-3′) were used for transcribing cDNAs of both polarities (50, 51). The forward primer was used to transcribe cDNA from the negative-strand RNA, whereas the reverse primer was used to transcribe cDNA from positive-strand RNA by using Improm II reverse transcription system (Promega). 40 ng of cDNA was used for real time RT-PCR analysis of viral RNA in Bio-Rad iQ-5 real time thermal cycler with the use of SYBR Green supermix (Bio-Rad) with the appropriate primer pair for either negative-strand (forward 5′-GGCCGTCATGGTGGCGAATAA-3′ and reverse 5′-CCATTTGCAGCAACACCATCTC-3′) or positive-strand (forward 5′-GGCCGTCATGGTGGCGAATAA-3′ and reverse 5′-CAGGCTATGGCACTGTCACGAT-3′) detection. The underlined sequence corresponds to the 5′-tagged sequence (51). Absolute positive- and negative-strand copy numbers were quantitated and reported as described above.

For extracellular viral RNA quantification, viral RNA from the supernatant was extracted by Qiagen viral RNA extraction kit according to the manufacturer's instructions, and for its quantification, a SYBR Green one-step real time RT-PCR (Bio-Rad) was conducted using the same PCR conditions as cellular RNA quantification, with primers that bind to the NS1 gene (as mentioned above). Absolute viral RNA genome copy was calculated based on the DENV standard curve generated and reported as absolute number of viral RNA genome copy per ml of supernatant. The detection limit of each real time RT-PCR assay is indicated as a gray line in the graph.

IFA against E protein by anti-E mouse antibody 4G2, NS3 protein by anti-NS3 human antibody 3F8, and dsRNA by anti-dsRNA mouse antibody J2 (Scicons), and Western blot against NS3 protein by anti-NS3 3F8 were performed as described previously (33). IFA images were captured on an inverted fluorescence microscope (Olympus IX71, Center Valley) at ×20 magnification, and image analysis was performed with ImageJ software (52).

Statistical Analysis—Student's *t* test was used to determine statistical significance. *p* values of ≤0.05 were considered as significant.

RESULTS

NS3(566–618) Interacts with NS5 RdRP—Even though NS3(303–618) of the helicase domain (residues 172–618, see Fig. 1*A*) was previously shown by Y2H study to interact with NS5(320–368) (bNLS) (36) of the RdRP domain (residues 273–900) (35, 36), the amino acid residues of NS3 helicase that are responsible for binding to NS5 RdRP have not been pinpointed. However, it was hypothesized that helicase subdomain III, NS3(482–618), contains the interaction site (13, 22). To test this, we first established that the binding of $NS2B_{18}NS3$ to coated NS5 RdRP increased in a dose-dependent manner as described previously (33) and carried out the NS3-NS5 interaction assay in a competitive ELISA format, with an increasing amount of the following competing proteins, namely NS3(172–618), GST-NS3(482–618) (subdomain III, or GST-NS3(566–618) (Fig. 1, *A* and *B*). From these data, all three NS3 truncated proteins were found to be able to compete with $NS2B_{18}NS3$ protein binding to coated NS5 RdRP (Fig. 1*C*). The apparent K_d values of the NS3-NS5 interaction for NS3(172–618), GST-NS3(482–618), and -(566–618) were found to be comparable (5.33 ± 0.35, 10.18 ± 0.91, and 10.25 ± 1.14 μM (mean ± S.D., $n = 3$) respectively) and also similar to the K_d values for NS3(172–618) as in previous reports (33, 37). Next, we also determined the IC_{50} value for NS3(172–618), which was 6.07 ± 2.60 μM. The IC_{50} values for GST-NS3(482–618) and GST-NS3(566–618) were not determined as we were unable to reach 100% inhibition due to limited availability of truncated protein. Protein expression constructs spanning other NS3 subdomain regions (NS3(172–482), -(307–619), and (172–566)) were also generated in this study, but due to protein stickiness, protein instability, or low protein yield, these proteins could not be purified to sufficient quantity for the competition assay.

NS3 Asn-570 Is Critical for the Interaction—To map the NS3 sequence that interacts with NS5 more precisely, we proceeded to screen an array of overlapping 15-mer peptides (Mimotopes) (53, 54) that spanned subdomain III in the same competitive ELISA format (Fig. 2*A*), and we identified two peptides (NS3(566–580) and -(571–585)) that moderately (p value = 0.06 and 0.009, respectively) blocked NS3-NS5 interaction, thus narrowing down the interaction region to residues 566–585 of NS3. We next tested the synthetic peptide NS3(566–585) in ELISA and showed that it could also disrupt NS3-NS5 interaction in a dose-dependent manner with an IC_{50} value of 128.8 ± 2.57 μM (Fig. 2*B*). At the same time, another peptide, NS3(86–100) with a similar charge as NS3(566–585), did not compete. This indicates NS3-NS5 interaction involves sequence-specific residues on the NS3 protein. Additionally, the same peptide also inhibited NS3-NS5 interaction in the AlphaScreen assay format where the interacting partners were synthesized *in vitro* using the wheat germ expression system (data not shown) (55).

Next, we also used the peptide in the viral inhibition assay to determine whether blocking the interaction site could reduce viral replication (Fig. 2*C*). Uptake of NS3(566–585) peptide into infected cells was facilitated by a well characterized cell-penetrating peptide, penetratin (56), which forms a nonconva-

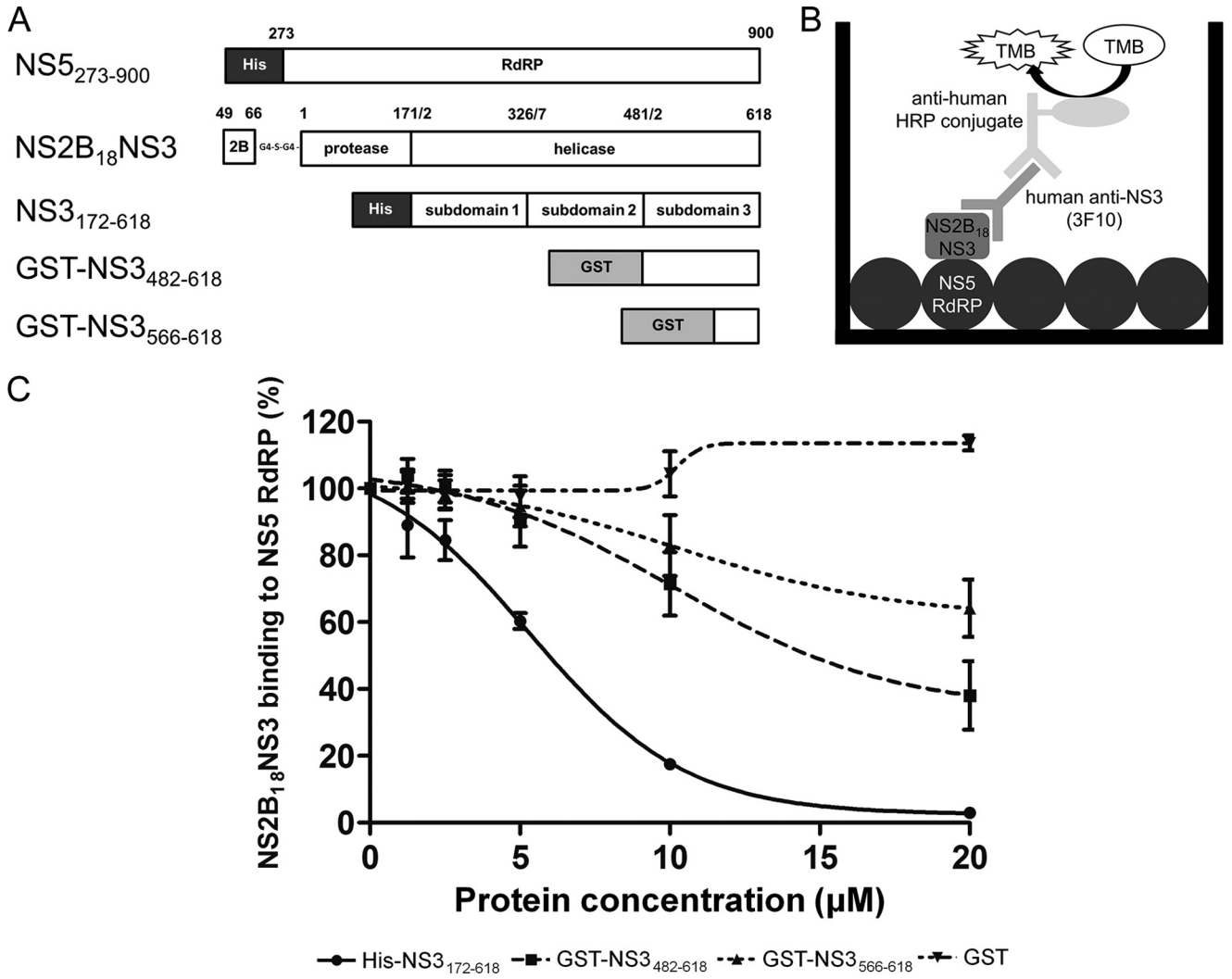

FIGURE 1. **Competitive NS3-NS5 interaction ELISA with NS3-truncated proteins.** *A*, schematic representation and diagram of the recombinant NS3 and NS5 proteins that were expressed in *E. coli* and used in *B* for competitive NS3-NS5 interaction ELISA. *C*, during incubation of $NS2B_{18}NS3$ protein with coated NS5 RdRP, 2-fold serial dilution of either NS3 or GST protein (starting from 20 μM) was added in triplicate competition experiments. GST protein was included as negative control. Data are shown as the mean ± S.D. of triplicates from two independent experiments.

lent complex with the peptide (57). As shown in Fig. 2*C*, NS3(566–585) peptide could reduce viral replication by ~33% (p value = 0.0195, Fig. 2*C, panel i*). As a positive control, we also tested the NS5(320–341) peptide that was covalently linked to penetratin, which can also facilitate the uptake of the peptide into infected cells (58). NS5(320–341) peptide could also reduce viral replication by ~33% (p value = 0.0043, Fig. 2*C, panel ii*). This suggests that blocking interaction between NS3 and NS5 could be a potential therapeutic target.

Sequence alignment of NS3(566–585) of DENV1–4 and other flaviviruses (Fig. 2*D*) suggested that Asn-570 (highlighted in *gray*) is highly conserved within this region and may be critical for the NS3-NS5 interaction. To test this, we synthesized NS3(566–585)(N570A) peptide and carried out the same competitive ELISA. We found that the replacement of asparagine by alanine at position 570 of NS3 resulted in a null-peptide with respect to its ability to block the NS3-NS5 interaction (Fig. 2*B*). Next, we expressed and purified the NS3:N570A full-length protein to measure its ATPase activity (59), and we found that it was comparable with the WT NS3 protein (Fig. 2*E*). The affinity of ATP for NS3 WT and NS3 N570A was similar (K_m = 185.8 ± 10.86 and 176.1 ± 8.73 μM, respectively). Both proteins also had similar turnover numbers (k_{cat} = 3.15 and 3.11 s^{-1}, respectively). From these results, we surmised that Asn-570 of NS3 helicase subdomain III appears to be critical for the NS3-NS5 interaction without affecting the *in vitro* ATPase activity.

NS5(320–341) of RdRP bNLS Binds to NS3 Helicase in Solution—To gain some insights on the NS3-NS5 interaction at the structural level, we constructed a synthetic fusion of NS3(172–618) with NS5(320–341) (within bNLS) connected by a flexible linker (G_4SG_4, NS3(172–618)-NS5(320–341); Fig. 3*A*) for SAXS study. NS5(320–341) was selected based on surface plasma resonance data for peptide binding and NS5 peptide-phage ELISA that supported the interaction of NS5(320–341) to NS3(172–618) (data not shown). Through modifications of the purification strategy, NS3(172–618) and NS3(172–618)-NS5(320–341) were purified to high purity and used in the SAXS experiments, which provide three-dimensional low resolution structures in solution (60) as described for single proteins (41, 61, 62), as well as multidomain complexes

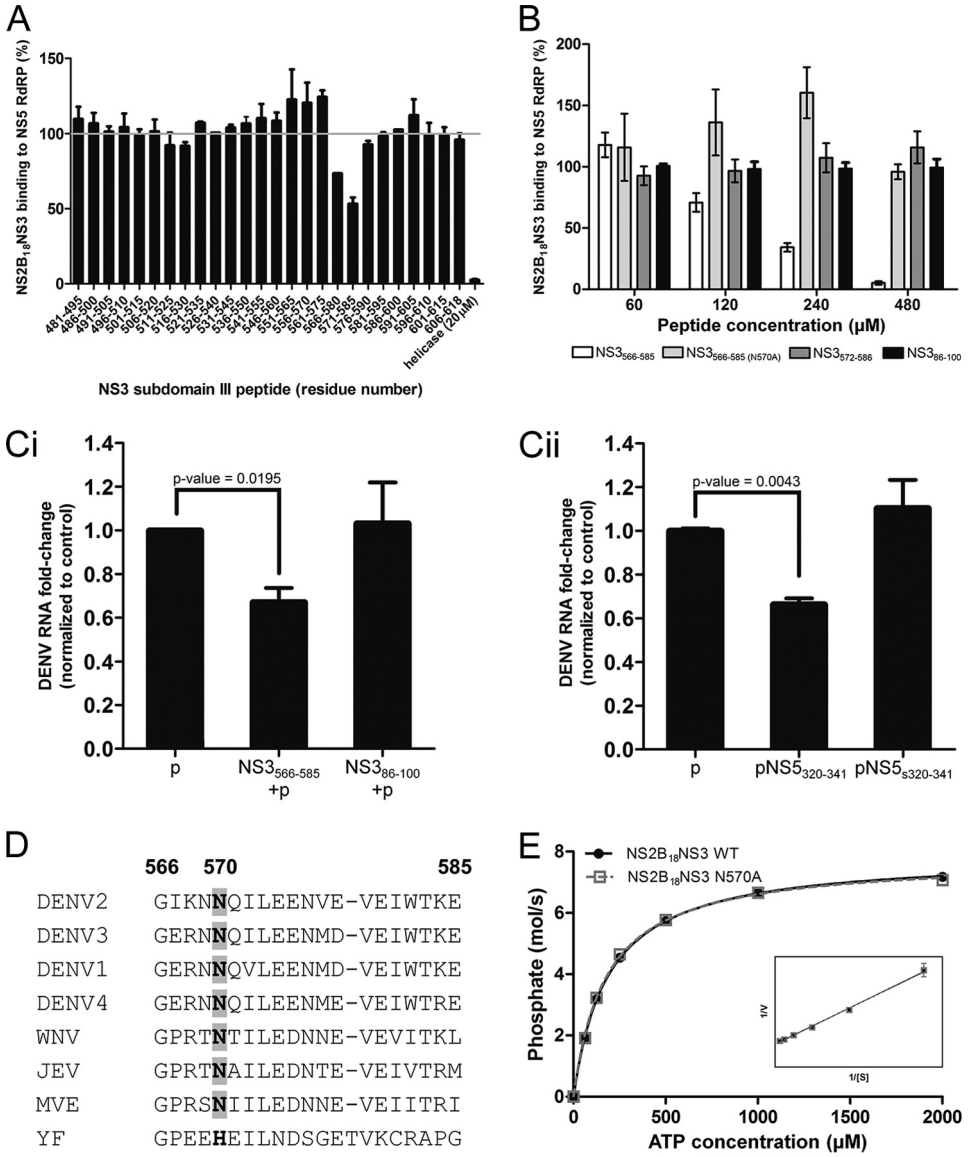

FIGURE 2. ***In vitro* functional characterization of NS3 residue Asn-570.** *A,* array of overlapping 15-mer peptides that spanned subdomain III were tested in the competitive ELISA as in Fig. 1*B*. 20 μM helicase was included as negative control and is shown as the mean ± S.D. of duplicates from one experiment. *B,* 2-fold serial dilution of 20-mer NS3(566–585) or NS3(566–585)(N570A) peptide (starting from 480 μM) was tested in the competitive ELISA as shown in Fig. 1*B*. NS3(86–100), which has a similar net charge as NS3(566–585) and NS3(571–585), was included as negative control. Data are shown as the mean ± S.D. of triplicates from two independent experiments. *C,* viral inhibition assay was performed with NS3 (*panel i*) or NS5 (*panel ii*) peptide that spanned the NS3-NS5 interaction site. For NS3 peptides, they formed a nonconvalent complex with penetratin peptide, which also enables NS3 peptide to be transported into the cells (57). For NS5 peptides, they were synthesized as penetratin fusion peptide as penetratin has been shown to have cell-penetrating property (73), and this enables the NS5 peptide to be transported into the cells. 6 h post-infection, the cells were treated with the peptides. Infected cells were harvested at 24 h post-infection for cellular viral RNA quantification by real time RT-PCR analysis. Fold-change was normalized to 24-h control (penetratin alone) and was plotted, and data are shown as the mean ± S.D. of duplicate from one independent experiment. The *x* axis labels are as follows: penetratin (*p*), penetratin and NS3(566–585) complex ($NS3_{566-585}+p$), and penetratin and NS3(86–100) complex ($NS3_{86-100}+p$) for *panel i* and penetratin (*p*), penetratin fused to NS5(320–341) ($pNS5_{320-341}$), and penetratin fused to scrambled NS5(320–341) ($pNS5_{s320-341}$) for *panel ii*. *D,* sequence alignment of NS3 residues 566–585 of DENV2 with other DENV serotypes and representative members of the *Flavivirus* genus (74). NS3 residue Asn-570 that is critical for NS3-NS5 interaction is highlighted in *gray* and *bold*. The alignment was performed using ClustalW (74). The virus sequences and their GenBank™ accession numbers are as follows: DENV2 (AF038403), DENV1 (U88535), DENV3 (M93130), DENV4 (AF326573), yellow fever virus (*YFV*; X15062), Japanese encephalitis virus (*JEV*; M55506), Murray Valley encephalitis virus (*MVEV*; AF161266), and West Nile virus (*WNV*; M12294). The numbering of residues is based on DENV2 protein sequence. *E,* ATPase assay of $NS2B_{18}$NS3 WT and N570A proteins was carried out with 2.5 nM protein, in the presence of the indicated concentrations of ATP. The amount of inorganic phosphate released during reaction was measured with the malachite green reagent, and the initial rates were computed (moles of phosphate released/s). The data points were fitted using Michaelis-Menten Equation 1 (see under "Experimental Procedures").

like ATPase (63, 64) and the NS3 protease-helicase complex of DENV (11). SAXS data of both proteins at three different concentrations were collected to yield the final composite scattering curves shown in Fig. 3, *B* and *C*, which indicate that both proteins are monodispersed in solution. Inspection of the Guinier plots at low angles revealed good data quality and no protein aggregation (Fig. 3, *B* and *C, insets*). NS3(172–618) has a radius of gyration (R_g) of 25.16 ± 0.6 Å and a maximum dimension (D_{max}) of 72.95 Å (Fig. 3*D*), whereas the NS3(172–618)-NS5(320–341) has an R_g of 25.42 ± 0.6 Å and a D_{max} of 75.64 Å (Fig. 3*D*). Comparison of the forward scattering of both proteins with the values obtained from a reference solution of

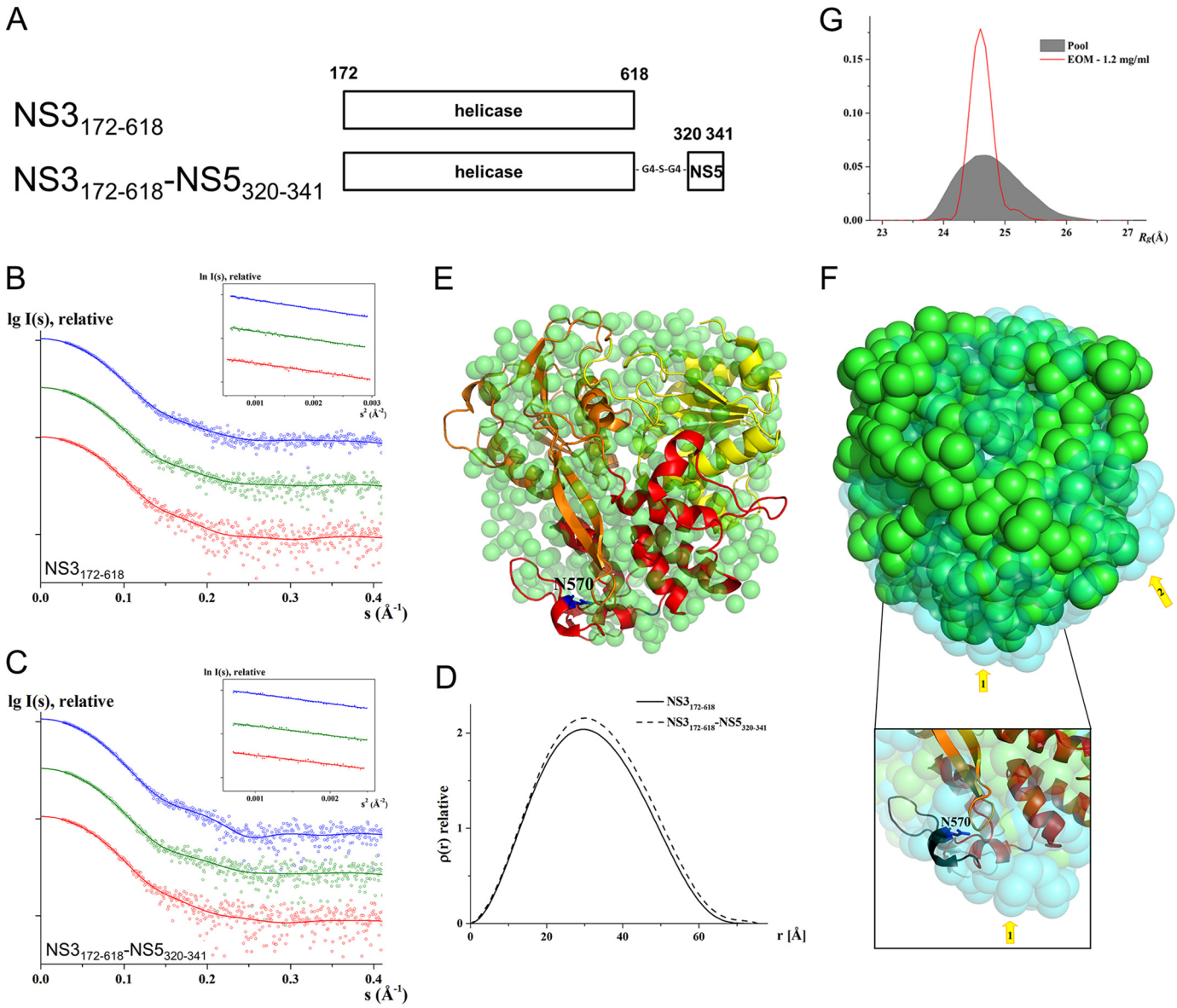

FIGURE 3. **SAXS of NS3(172–618)-NS5(320–341) indicates NS3-NS5 interaction.** *A,* schematic representation of recombinant NS3 and NS3-NS5 fusion proteins that were expressed in *E. coli* and used in SAXS study. SAXS scattering pattern (○) and its corresponding experimental fit (—) of NS3(172–618) (*B*) and NS3(172–618)-NS5(320–341) (*C*) at protein concentrations of 1.2 mg/ml (*red*), 2.1 mg/ml (*olive*), and 4 mg/ml (*blue*). The curves are displayed in logarithmic unit for clarity. The *insets* in *B* and *C* show the respective Guinier plot. *D,* distance distribution functions of NS3(172–618) (—) and NS3(172–618)-NS5(320–341) (—). *E,* superposition of the determined solution shape of NS3(172–618) with the crystallographic structure of NS3(172–618) (Protein Data Bank code 2JLS (12)). Subdomains I, II, and III are colored in *yellow, orange,* and *red*, respectively. *F,* superposition of the NS3(172–618) and (*green*) and NS3(172–618)-NS5(320–341) (*cyan*) solution shapes. The R_g of the NS3(172–618) and NS3(172–618)-NS5(320–341) is 25.2 and 25.4 Å, respectively. The *arrows* indicate the two protrusions, one at the bottom of the NS3(172–618)-NS5(320–341) solution shape, which leads to a more elongated shape in this protein, reflected by the increased D_{max} value (see Fig. 3*D*). This protrusion is in proximity to the Asn-570 (*blue sticks*) and NS3 peptide region, NS3(566–585) (*black schematic*) (*inset* in *F*). The second protrusion of the NS3(172–618)-NS5(320–341) may be caused by a conformational alteration due to NS3(172–618) and NS5(320–341) interactions. *G*, EOM R_g distribution of the selected ensemble (*red line*) contains a narrow peak at 24.6 Å, which is slightly smaller than the center R_g of the random pool (*gray filled area*), 24.8 Å, suggesting NS3(172–618)-NS5(320–341) is rigid and compact in solution, and peptide NS5(320–341) is bound to NS3(172–618).

lysozyme (14.4 kDa) yielded a molecular mass of 44.4 kDa for NS3(172–618) and 47.7 kDa for NS3(172–618)-NS5(320–341), indicating that both proteins are monomeric at the concentrations used.

The low resolution solution structures of NS3(172–618) and NS3(172–618)-NS5(320–341) were restored *ab initio* using the program GASBOR (45). The normalized spatial discrepancy (NSD) of 10 independent reconstructions of NS3(172–618) is 0.95 ± 0.02 Å, and the NSD of 10 reconstructions of NS3(172–618)-NS5(320–341) is 0.99 ± 0.03 Å. The reconstructions with the least NSD from both proteins were selected, and the obtained solution shapes for both proteins yielded a good fit to the experimental data in the entire scattering range. The corresponding fits for NS3(172–618) and NS3(172–618)-NS5(320–341) have discrepancies of $\chi = 1.15$ and $\chi = 1.04$, respectively. NS3(172–618) and NS3(172–618)-NS5(320–341) revealed globular shapes, with the dimensions of about 59.9 × 54.4 × 34 and 65.6 × 57.7 × 36.8 Å, respectively. When superimposed, the crystallographic structure of NS3(176–618) (Protein Data Bank code 2JLS) accommodated very well in the

solution form of the protein (Fig. 3*E*), indicating the high quality of the solution data. When the solution form of NS3(172–618) (*green*) and NS3(172–618)-NS5(320–341) (*cyan*) were superimposed (Fig. 3*F*), two protrusions were observed and are denoted by *arrows* in Fig. 3*F*. Protrusion 1 that is at the bottom of the NS3(172–618)-NS5(320–341) solution shape leads to a more elongated conformation in NS3(172–618)-NS5(320–341) than NS3(172–618). This is also reflected by the increased D_{max} in NS3(172–618)-NS5(320–341) (75.64 Å) when compared with the D_{max} of NS3(172–618) (72.95 Å) (Fig. 3*D*). The protrusion is in close proximity to residue Asn-570 (shown as *blue sticks* in the *inset* of Fig. 3*F*) and to the NS3 peptide region, NS3(566–585) that used in ELISA (shown as *black schematic* in the *inset* of Fig. 3*F*). The arrangement of NS3(566–585) enables an interaction with NS5(320–341) to occur.

Comparison of the NS3(172–618) and NS3(172–618)-NS5(320–341) low resolution structures also revealed a second protrusion of the NS3(172–618)-NS5(320–341) that may reflect a conformational alteration due to the NS3(172–618) and NS5(320–341) interaction. Taken together, these results appear to be consistent with the ELISA data and suggest a physical interaction between NS3(172–618) and NS5(320–341) in solution.

To eliminate the possibility that the peptide may be flexible in solution, the x-ray scattering data set of NS3(172–618)-NS5(320–341) had been further analyzed using the Ensemble Optimization Method (EOM) (47, 48) to assess the compactness and flexibility of NS3(172–618)-NS5(320–341) in solution. Based on the width and position of the selected ensemble peak relative to random pool in R_g distribution, the flexibility and compactness of the protein in solution can be determined. In the case of NS3(172–618)-NS5(320–341), the R_g distribution of the ensemble contains a narrow peak, indicating that NS3(172–618)-NS5(320–341) is rigid in solution. This peak is centered at 24.6 Å, which is slightly smaller than the center R_g of a random pool, 24.8 Å, suggesting that NS3(172–618)-NS5(320–341) is compact in solution. The EOM data demonstrate that peptide NS5(320–341) is bound to NS3(172–618).

NS3:N570A Mutant Has Reduced Infectious Virus Production and Viral Protein Synthesis—To study the impact of NS3:N570A mutation on NS3-NS5 interaction during the virus life cycle, we first generated a DENV2 WT cDNA clone by standard molecular cloning techniques. DENV2 of strain D2/SG/05K3295DK1/2005 of the cosmopolitan genotype (GenBank™ accession number EU081177.1) was isolated during a local dengue outbreak that occurred in 2005 as part of Early Dengue Infection and Outcome (EDEN) Study in Singapore, and it was picked as the template for construction of the DENV2 full-length cDNA clone because of the well documented history of the patients (38). The overall schematic representation of cloning strategy is shown in Fig. 4*A*. The cDNA clone was subdivided into three fragments based on unique restrictions that are present within the genome to facilitate the assembly of the full-length clone. To prevent unwanted rearrangement of the clone, both full-length cDNA and cDNA fragments were maintained in low copy plasmid pWSK29 and *E. coli* XL-1 Blue that were transformed with these plasmids grown at 30 °C (49). The assembled full-length cDNA clone contained a T7 promoter at the 5′ end for *in vitro* transcription and a SacI site at the 3′ end for linearization of cDNA. The use of SacI site generated the *in vitro* RNA transcript, which contains an additional nonviral nucleotide at the 3′ end, instead of two additional nonviral nucleotides for DENV cDNA that used the XbaI site (65). Prior to linearization for *in vitro* transcription, the full-length cDNA was checked for possible rearrangement by EcoRI digestion, and the predicted fragments of 9609, 4015, 1284, and 1122 bp were observed on 0.6% agarose gel (data not shown), indicating no sign of recombination (65).

IFA of BHK-21 cells that were transfected with *in vitro* transcribed genome-length RNA showed increasing numbers of cells expressing E protein from days 1 to 3 post-transfection, with ~50–60% of cells being E-positive on day 3 (Fig. 4*B*). Plaque assay for supernatant showed an increase in infectious viral particles from days 1 to 3, peaking at 1×10^5 pfu/ml on day 3 (Fig. 4*C*). The size of the plaque on BHK-21 cells, which was produced by the supernatant of BHK-21-transfected cells, was comparable with those produced by the supernatant of C6/36-transfected cells (Fig. 4*C, left* and *right insets,* respectively). These results show that the RNA transcribed from the cDNA clone is highly infectious and that infectious virus can be produced in both BHK-21 mammalian cells and C6/36 mosquito cells.

After determining the growth kinetics of cDNA clone-derived DENV2 WT virus, the DENV2 NS3:N570A cDNA mutant clone was generated by site-directed mutagenesis, and its phenotype in infectious virus production and viral protein synthesis was examined over the course of 5 days' post-transfection. For comparison, we also generated the NS5:K330A mutant (37), a known NS3-NS5 interaction-defective mutant that failed to replicate by reverse genetics studies, as a control. Similar to the NS5:K330A mutant, no infectious virus was recovered from the NS3:N570A mutant even when neat supernatant was used for titering (Fig. 5*B*). In agreement with the lack of infectious virus, extracellular viral RNA levels for both mutants were at the limit of detection of DENV RNA by RT-PCR and did not change over 5 days, suggesting that the mutants are inviable (Fig. 5*A*). The RNA detection for WT increased over 72 h when it reached maximal virus RNA detection that stabilized until 120 h. Next, to determine whether polyprotein synthesis from the transfected RNA is occurring and that the absence of infectious virus particles may be due to a lack of packaging and/or release of infectious virion, we checked the level of NS3 protein by both Western blot and IFA. Surprisingly, for the cells transfected with NS3:N570A mutant transcript, we could detect NS3 protein using humanized monoclonal antibody 3F8 (33) in the 24- and 48-h samples (Fig. 5*C, red arrows*) but not in the 72-h sample. The highest percentage of NS3-positive cells (5–10%) was observed on day 2 post-transfection, which declined to ≤5% of NS3-positive cells on day 3 post-transfection (Fig. 5*D*), and finally to an undetectable level at later time points on days 4 and 5 (data not shown). On the other hand, for the NS5:K330A mutant, the NS3 protein was almost undetectable by Western blot and IFA (≤1% of NS3-positive cells) at all time points post-transfection (Fig. 5, *C* and *D*). Taken together, the results indicate that reduced NS3-

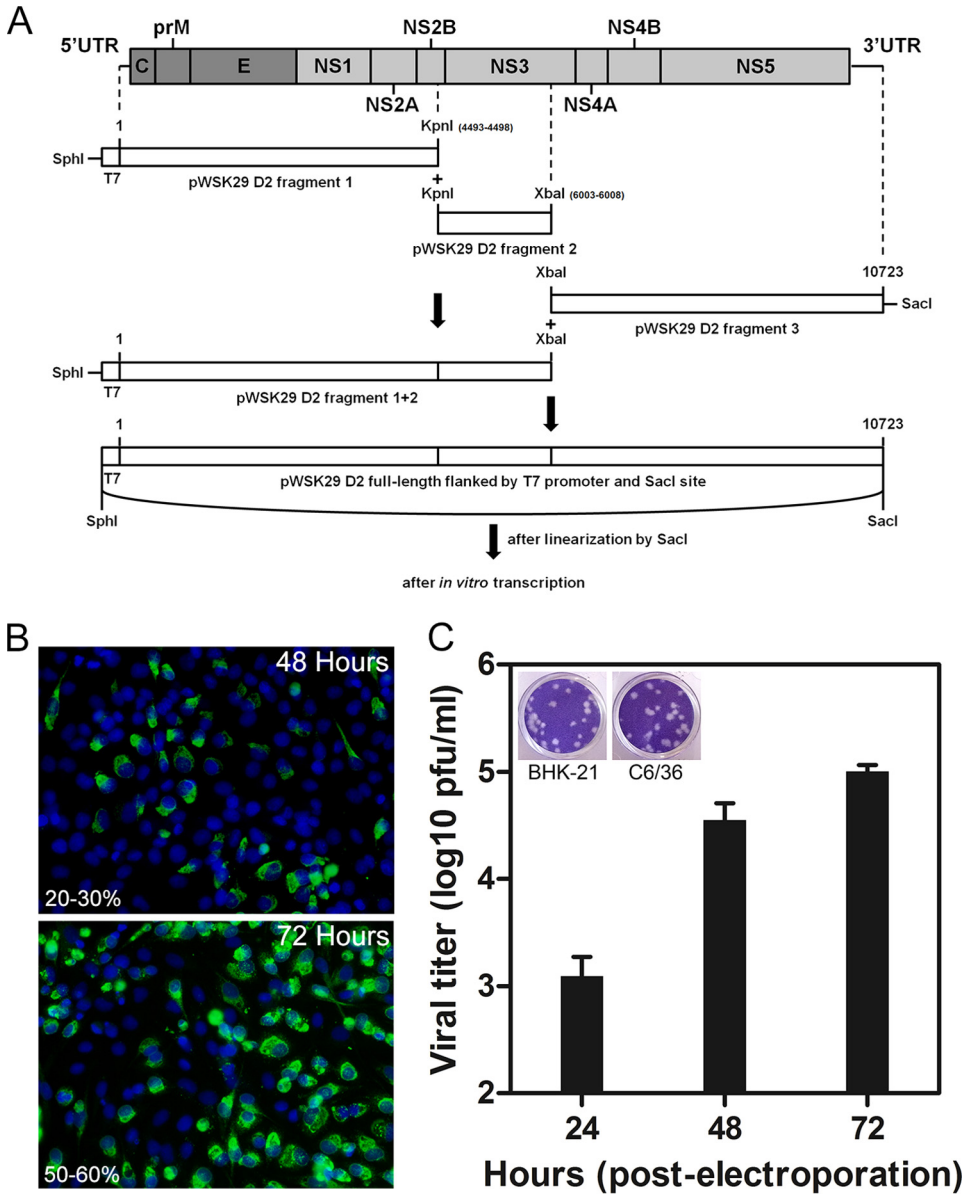

FIGURE 4. **Construction of DENV2 cDNA infectious clone.** *A,* schematic representation of full-length DENV2 cDNA clone generation. The DENV genome (represented approximately to scale) contains a single open reading frame that encodes three structural proteins (c, premembrane protein, and *E*) and seven NS proteins (NS1, NS2A, NS2B, NS3, NS4A, NS4B, and NS5). Three fragments (fragment boundaries indicated by nucleotide numbers) covering the entire viral genome were made and digested using unique restriction sites to facilitate the assembly of full-length cDNA clone (refer to "Experimental Procedures" for details). The complete DENV2 clone has a T7 promoter at 5′ end for *in vitro* transcription and SacI site at 3′ end for linearization of plasmid. *B* and *C,* BHK-21 cells were electroporated with 10 μg of genomic length RNA, and samples were harvested daily for 3 days. *B,* infected cells were analyzed for the presence of E protein by IFA with mouse anti-E 4G2 antibody on 48 and 72 h post-transfection, and percentage infection was determined. *C,* culture supernatants were used to determine viral titer by plaque assay on BHK-21 cells. The size of plaque on BHK-21 cells that was derived from the supernatant of either BHK-21 (*left inset*) or C6/36 (*right inset*) cells, which was transfected with DENV2 WT RNA, is shown.

NS5 interaction in NS3:N570A mutant impairs infectious virus production and viral protein synthesis.

NS3:N570A Mutant Showed Accumulation of Negative-strand RNA—The reduction in viral protein synthesis for the NS3:N570A mutant and the lack of detectable infectious plaques suggest that attenuated RNA replication could occur at an early time point for this mutant. Therefore, we examined the RNA replication kinetics by real time RT-PCR and IFA for detection of dsRNA. The results showed that intracellular RNA can be detected for NS3:N570A and WT but, intriguingly, not for NS5:K330A-transfected cells (Fig. 6*A* and *B*). The RNA copy for WT increased from around 10^6 copies/μg at 6 h post-transfection to 10^9 copies/μg of RNA at 120 h, as detected by real-time RT-PCR. Although less than WT, a 10-fold increase in intracellular viral RNA copy was observed from day 1 to 2 (p value = 0.008) for NS3:N570A mutant and thereafter, the level declined till day 5. The RNA copy for the NS5:K330A mutant declined from 6 to 48 h post-transfection and remained relatively stable from 48 to 120 h, suggesting that there was no viral RNA replication, and only the input RNA that was transfected by electroporation was being detected. Interestingly, the detection of the peak intracellular RNA level for NS3:N570A mutant on day 2 correlated with the highest level of NS3 protein detected by Western blotting (Fig. 5*C*).

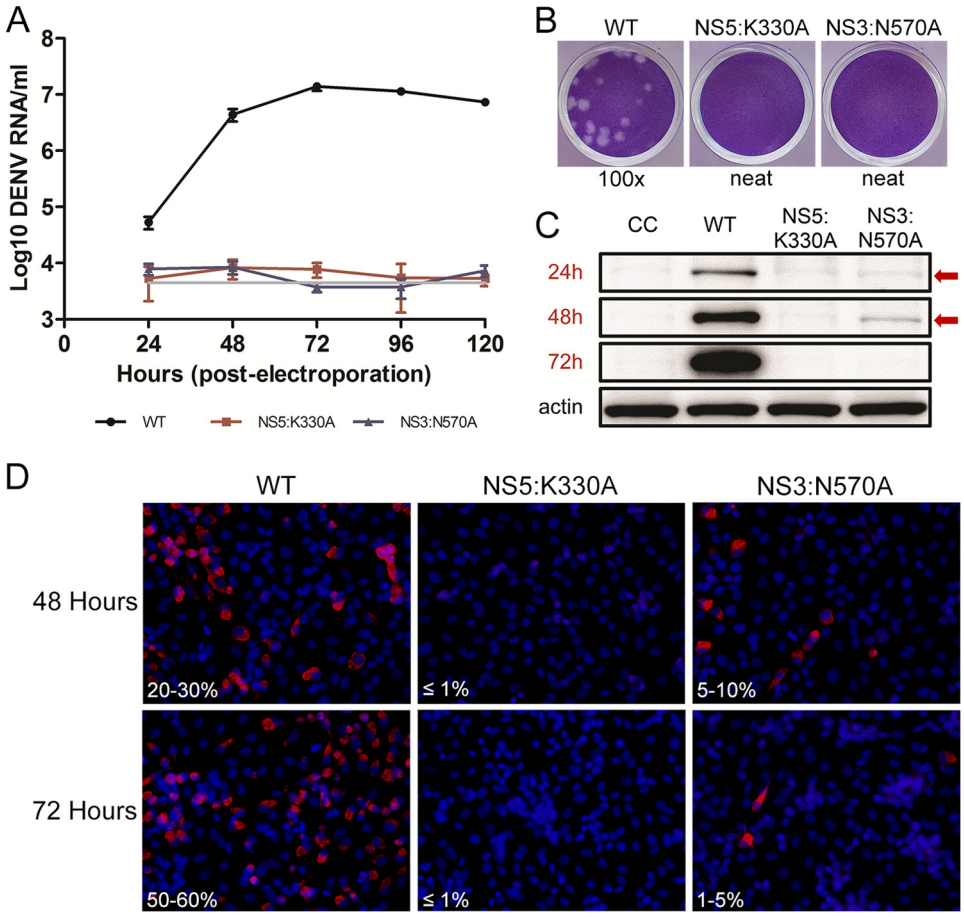

FIGURE 5. **Real time RT-PCR and plaque assay of supernatant, and Western blot and IFA against NS3 proteins of cells transfected with DENV2 WT, NS5:K330A, or NS3:N570A RNAs.** *A–C,* BHK-21 cells were electroporated with 10 μg of WT and mutant (NS3:N570A and NS5:K330A as control) genomic length RNA, and samples were harvested daily for 5 days. Culture supernatants were used to determine the absolute number of extracellular viral RNA copy by real time RT-PCR (*A*) and to check for plaque production on BHK-21 cells (*B*). Data are shown as the mean ± S.D. of duplicates from two independent experiments. Plotted absolute number of viral RNA copy in log scale per ml of supernatant used for real time RT-PCR is shown. The detection limit of real time RT-PCR assay is indicated as a *gray line* in the graph. *C* and *D*, Western blot (*C*) and IFA against NS3 protein (*D*) were performed with the use of human anti-NS3 3F8 antibody (33), and one representative experiment out of two independent studies was shown.

To explore this further, we quantified the level of intracellular positive- and negative-strand viral RNA with strand-specific tagged primers in the real time RT-PCR experiment (Fig. 6*C*). Essentially, the tag sequence that was described by Plaskon *et al.* (51) was fused to the sequence that binds to E gene (50) to create a primer that can bind to either the positive or negative strand during the cDNA synthesis step. During real time RT- PCR, the tag and E-specific primers were used to distinguish cDNAs that were transcribed from either the positive- or negative-strand template for accurate quantification of both strands. As expected, for WT viral RNA-transfected cells, the level of both positive- and negative-strand RNAs increased over time until day 3 and declined at slightly different rates after that until day 5. The quantification was consistent with previous data that an excess of positive- over negative-strand RNA can be detected in WT virus-infected cells (66). The RNA quantification for the NS3:N570A mutant revealed a different trend to WT and NS5:K330A mutants. Overall, the level of positive- and negative-strand RNA synthesis for NS3:N570A was lower than WT. However, the level of negative-strand RNA synthesis (rate = $2.06 \times 10^4 \pm 9.77 \times 10^2$ negative-strand/h) for NS3:N570A appeared to increase faster than positive-strand RNA (rate = $-2.17 \times 10^5 \pm 5.82 \times 10^4$ positive-strand/h) during a 6–24-h period, and at a somewhat similar rate for both strands (rate = $3.55 \times 10^5 \pm 3.74 \times 10^3$ negative-strand/h and $7.48 \times 10^5 \pm 1.28 \times 10^5$ negative-strand/h) during the 24–48-h period, suggesting that the negative-strand RNA may be accumulating as a double-stranded replicative form by base-pairing with the transfected positive-sense RNA. Interestingly, beyond 48 h, the rates at which both positive- and negative-strand RNA accumulated for NS3:N570A mutant over time were almost identical. For NS5:K330A mutant, the level of detected positive- and negative-strand RNA corresponds to the amount of transfected positive- and negative-strand RNA that degraded over time. (Note: T7 transcribed positive-sense RNA used for transfection contained ~0.1–0.3% negative-sense RNA that could be detected by the primers that bind to E gene and is the basis for the *gray* cutoff line for the residual negative-strand from transfected RNA in Fig. 6*C*.) The NS3:N570A mutant probably results in either reduced or completely abolished NS3-NS5 interaction and does not support further RNA synthesis from the dsRNA template that is formed (67). This is consistent with the detection of highest percentage of dsRNA-positive cells on day 2 (5–10%) by intracellular RNA staining that does not accu-

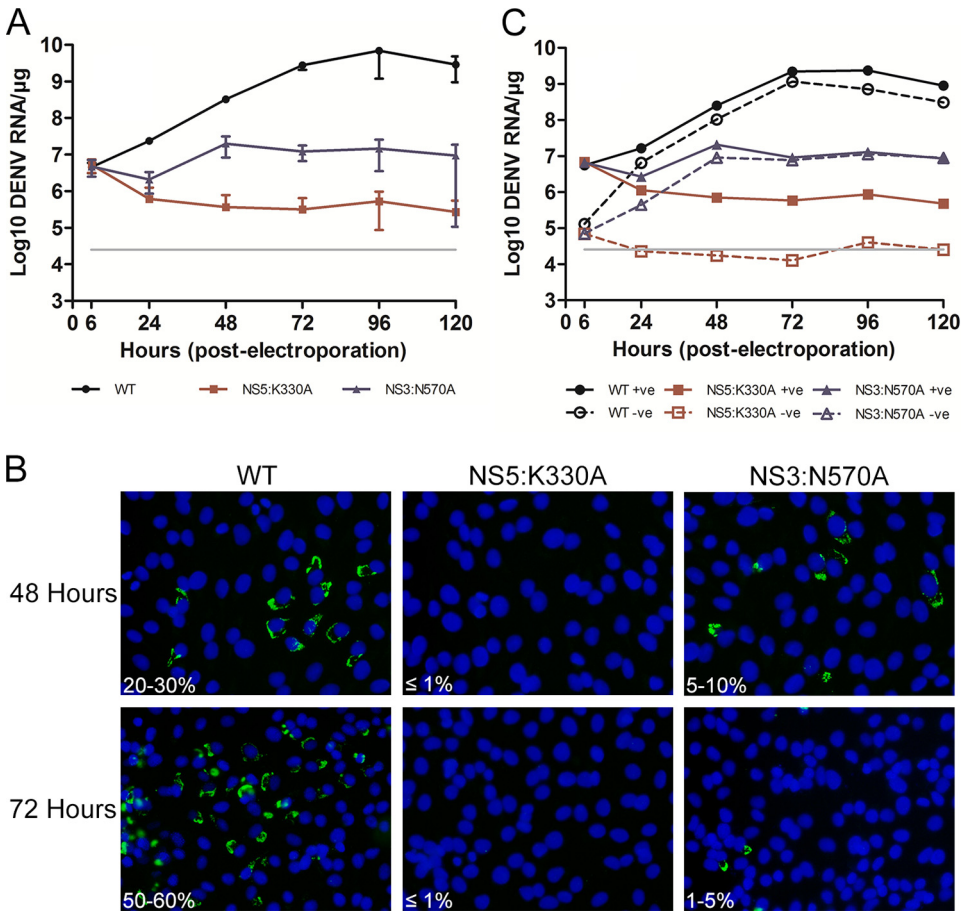

FIGURE 6. **Real time RT-PCR and IFA against dsRNA of cells transfected with DENV2 WT, NS5:K330A, or NS3:N570A RNAs.** *A–C,* same experiment setup was performed as mentioned in Fig. 5. *A,* RNA was extracted from infected cells, and the absolute number of intracellular viral RNA copy was determined by real time RT-PCR. *B,* infected cells were analyzed for the presence of dsRNA by IFA with mouse anti-dsRNA antibody on 48 and 72 h post-transfection, and percentage infection was determined. Data from one independent experiment are shown, and it is a separate experiment from Figs. 4*B* and 5*D*. *C,* extracted RNA was also used to determine positive- and negative-strand synthesis by real time RT-PCR, and absolute number of intracellular viral RNA copy was plotted (one independent experiment). Data are shown as the mean ± S.D. of duplicate from one independent experiment. Plotted absolute number of viral RNA copy in log scale per μg of RNA used for real time RT-PCR. The *gray line* in *A* and *C* indicates the amount of residual negative strand from transfected RNA.

mulate as seen in WT at the later time points (Fig. 6*B*). Interestingly, our detailed analysis suggests that NS5:K330A mutant cannot synthesize negative-strand RNA, although the mutation has been shown to have no effect on the *in vitro* enzymatic activities (37). These results suggest that the impairment of infectious virus production and viral protein synthesis in the NS3:N570A mutant may be due to the inability of the mutant NS3 to engage with NS5 and use the dsRNA template to produce more positive-strand genomic RNA that can be translated and processed.

DISCUSSION

Flavivirus NS3 and NS5 proteins are recognized as attractive targets for antiviral drug development because of their important functional roles in viral replication (68–71). Because of the potential interdependence of the two proteins in orchestrating viral genome replication in the RC, the interaction between NS3 and NS5 has been proposed as a promising new target (28, 29, 37, 71). It was previously demonstrated by the Y2H study that NS3(303–618) of the helicase domain interacts with NS5(320–368) of the RdRP domain. Subsequently, based on available crystal structures, subdomain III of NS3 helicase (residue 483–618) was suggested to be involved in the interaction with NS5 because it has a large protein surface area, located away from the region of main catalytic active sites of NS3 (13, 22, 36). The NS5 residue Lys-330, which is located on the surface of NS5 thumb subdomain, has been identified as a critical residue in interacting with NS3 helicase (37).

In this study, we focused our attention on identifying the NS3 residues involved in the NS3-NS5 interaction, and we used biochemical, genetic, and biophysical approaches to investigate the functional relevance of the proposed interaction site. Through the use of truncated NS3 protein constructs, overlapping peptides, and peptide phage display, we had fine-mapped the interaction region to residues 566–585 for NS3 and residues 320–341 for NS5. Our attempts to obtain crystals of NS3 and NS5 in complex were not successful, and therefore, we employed SAXS to obtain a solution shape that supports the physical interaction between NS3(172–618) and NS5(320–341). Through EOM analysis of the SAXS data, we were able to demonstrate that NS3(172–618)-NS5(320–341) is compact and rigid, indicating that peptide NS5(320–341) makes specific and discrete interactions with the helicase domain, NS3(172–618).

Electrostatic potential surface analysis of NS3(566–585) and NS5(320–341) shows a negatively charged contiguous surface

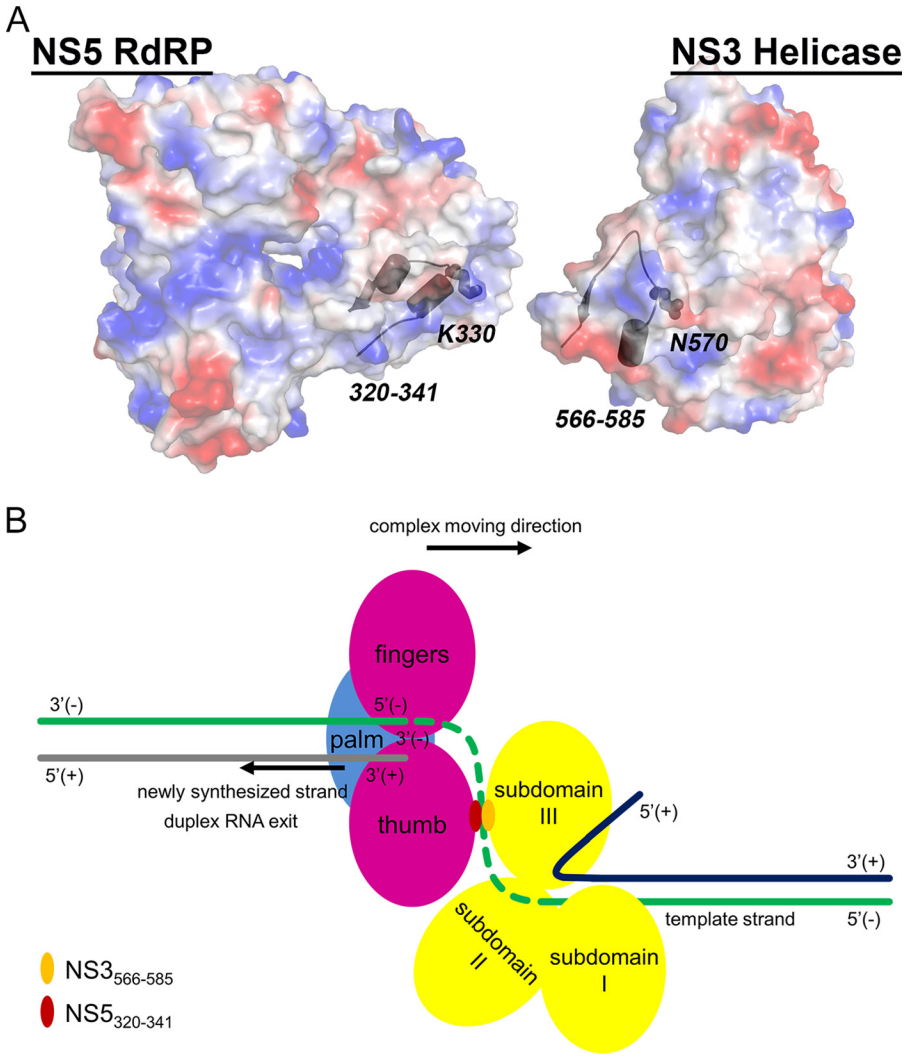

FIGURE 7. **Schematic representation of NS3-NS5-RNA interaction.** *A,* surface electrostatic potential presentation of NS5(273–900) (RdRP) and NS3(172–618) (helicase). The protein backbones of NS5(320–341) and NS3(566–585) are shown in *ribbon* presentation. The side chains of NS5 Lys-330 and NS3 Asn-570 are displayed. *B,* simplified schematic model of NS3-NS5 interaction complex with RNA. *Dashed line* (*green*) is used to denote that the uncertain path that exiting template RNA from NS3 takes to enter NS5 for complementary daughter strand synthesis. *Dark blue line* denotes the unwound parental strand; *green line* denotes the parental strand that serves as template; *gray line* denotes the newly synthesized daughter strand.

on NS3 and a positively charged contiguous surface on NS5, which are charge-complementary to each other, and this further supports the results that the two regions can indeed interact with one another via charge interaction (Fig. 7*A*). Inspection of the amino acid sequence in NS3(566–585) region within flavivirus (Fig. 2*D*) indicated a high conservation of sequence, and we identified a conserved amino acid within this region, residue Asn-570, which we showed to be important for NS3-NS5 interaction; the mutation of this residue to alanine disrupts the *in vitro* NS3-NS5 interaction. When the same mutation was engineered into the DENV2 cDNA clone, it abolished infectious virus production, similar to NS5:K330A mutant (37). However, unlike the NS5:K330A mutant, the NS3:N570A mutant was able to synthesize low but unsustainable amounts of viral RNA and proteins. Comparison of the pattern of positive- and negative-strand RNA synthesis between WT, NS3:N570A, and NS5:K330A confirmed that the NS5:K330A mutant is completely inactive since transfected positive-strand RNA degraded over time, and the negative-strand RNA detected corresponded to background. The WT RNA-transfected cells showed synchronized synthesis of positive- and negative-strand RNA, which is in agreement with previous studies that have shown an excess of positive- to negative-strand RNA in DENV-infected cells (66). However, it is possible that the long term coordinated synthesis of positive- and negative-strand RNA requires a functional RC with optimum protein interaction affinities between NS3 and NS5 (Fig. 7*B*). This is supported by the NS3:N570A mutant that showed fairly robust negative-strand synthesis using the transfected RNA as a template, and it is probably analogous to the situation at the early stages of viral replication in an infected cell. The weakened or abolished interaction between NS3 and NS5 in the NS3:N570A mutant does not support the replication of new positive-strand RNA from 6 to 24 h when compared with WT virus, which fits rather well with the carefully conducted real time RT-PCR quantifications. Surprisingly, the NS5:K330A mutant that has been shown to be enzymatically active *in vitro* and demonstrated to have no interaction with NS3 did not show a

similar increase in negative-strand RNA as compared with NS3: N570A mutant. There may be two possible reasons for the inactivity of the NS5:K330A mutant in making negative-strand RNA. First, it may be due to impaired intramolecular signaling between the two NS5 domains that probably coordinate the two functional activities of NS5 (72) required for *in vivo* polymerase activity. Second, its weak/abolished interaction with NS3 may affect the unwinding of secondary structures in the transfected positive-sense RNA that is needed for negative-strand synthesis. Taken together, our study indicates that different NS3-NS5 interaction-defective mutants can impair infectious virus production, viral protein synthesis, and RNA replication to varying degrees, which is likely to be dependent on the importance of the amino acids that are involved in NS3-NS5 interaction, and also possibly the intramolecular interactions in NS5. It is interesting to note that the coordinated synthesis of positive- and negative-strand RNA at the early stages of replication can be further explored by studying NS3-NS5 interaction mutants displaying varying strengths/degrees of binding and also the contribution of intramolecular cross-talk between the domains of NS5 in strand-specific RNA synthesis in the RC (Fig. 7*B*). Importantly, we also note that although the NS3 residue Asn-570 is conserved among the four DENV serotypes and several members of flavivirus genus, it is not conserved in yellow fever virus NS3, which has a histidine in place of asparagine at this position in NS3 and tyrosine instead of lysine at position 330 of NS5 (for sequence alignment, refer to Figs. 1*B* and 5 in Ref. 36).

Overall, this study has identified a potentially new druggable target for the development of antiviral drugs to block NS3-NS5 interaction that is essential for viral replication. The available crystal structures of NS3 and NS5 together with *in vitro* assays for interaction can be used for *in silico* and high throughput screening campaigns to find lead molecules for antiviral drug development. Alternatively, because the NS3:N570A mutant genome can be translated to a low level and is able to synthesize negative-strand RNA, it may serve as a potential RNA-mediated vaccine, although the basis for this requires development of new technology platforms.

Acknowledgments—We thank Drs. Mallur Madhusudhan, Chandrakala Basavannacharya, Yoichi Suzuki, Yin Hoe Yau, and Susana Geifman Shochat for valuable suggestions, discussion, and experimental assistance.

REFERENCES

1. Bhatt, S., Gething, P. W., Brady, O. J., Messina, J. P., Farlow, A. W., Moyes, C. L., Drake, J. M., Brownstein, J. S., Hoen, A. G., Sankoh, O., Myers, M. F., George, D. B., Jaenisch, T., Wint, G. R., Simmons, C. P., Scott, T. W., Farrar, J. J., and Hay, S. I. (2013) The global distribution and burden of dengue. *Nature* **496,** 504–507
2. Lindenbach, B. D., Thiel, H., and Rice, C. M. (2007) in *Fields Virology* (Knipe, D. M. and Howley, P. M., eds) 5th Ed., pp. 1101–1152, Wolters Kluwer/Lippincott Williams & Wilkins, Philadelphia
3. Bartholomeusz, A. I., and Wright, P. J. (1993) Synthesis of dengue virus RNA *in vitro*: initiation and the involvement of proteins NS3 and NS5. *Arch. Virol.* **128,** 111–121
4. Falgout, B., Pethel, M., Zhang, Y. M., and Lai, C. J. (1991) Both nonstructural proteins NS2B and NS3 are required for the proteolytic processing of dengue virus nonstructural proteins. *J. Virol.* **65,** 2467–2475
5. Preugschat, F., Yao, C. W., and Strauss, J. H. (1990) *In vitro* processing of dengue virus type 2 nonstructural proteins NS2A, NS2B, and NS3. *J. Virol.* **64,** 4364–4374
6. Wu, C. F., Wang, S. H., Sun, C. M., Hu, S. T., and Syu, W. J. (2003) Activation of dengue protease autocleavage at the NS2B-NS3 junction by recombinant NS3 and GST-NS2B fusion proteins. *J. Virol. Methods* **114,** 45–54
7. Zhang, L., Mohan, P. M., and Padmanabhan, R. (1992) Processing and localization of Dengue virus type 2 polyprotein precursor NS3-NS4A-NS4B-NS5. *J. Virol.* **66,** 7549–7554
8. Chambers, T. J., Nestorowicz, A., Amberg, S. M., and Rice, C. M. (1993) Mutagenesis of the yellow fever virus NS2B protein: effects on proteolytic processing, NS2B-NS3 complex formation, and viral replication. *J. Virol.* **67,** 6797–6807
9. Yon, C., Teramoto, T., Mueller, N., Phelan, J., Ganesh, V. K., Murthy, K. H., and Padmanabhan, R. (2005) Modulation of the nucleoside triphosphatase/RNA helicase and 5′-RNA triphosphatase activities of Dengue virus type 2 nonstructural protein 3 (NS3) by interaction with NS5, the RNA-dependent RNA polymerase. *J. Biol. Chem.* **280,** 27412–27419
10. Sampath, A., Xu, T., Chao, A., Luo, D., Lescar, J., and Vasudevan, S. G. (2006) Structure-based mutational analysis of the NS3 helicase from dengue virus. *J. Virol.* **80,** 6686–6690
11. Luo, D., Xu, T., Hunke, C., Grüber, G., Vasudevan, S. G., and Lescar, J. (2008) Crystal structure of the NS3 protease-helicase from dengue virus. *J. Virol.* **82,** 173–183
12. Luo, D., Xu, T., Watson, R. P., Scherer-Becker, D., Sampath, A., Jahnke, W., Yeong, S. S., Wang, C. H., Lim, S. P., Strongin, A., Vasudevan, S. G., and Lescar, J. (2008) Insights into RNA unwinding and ATP hydrolysis by the flavivirus NS3 protein. *EMBO J.* **27,** 3209–3219
13. Xu, T., Sampath, A., Chao, A., Wen, D., Nanao, M., Chene, P., Vasudevan, S. G., and Lescar, J. (2005) Structure of the Dengue virus helicase/nucleoside triphosphatase catalytic domain at a resolution of 2.4 A. *J. Virol.* **79,** 10278–10288
14. Matusan, A. E., Pryor, M. J., Davidson, A. D., and Wright, P. J. (2001) Mutagenesis of the Dengue virus type 2 NS3 protein within and outside helicase motifs: effects on enzyme activity and virus replication. *J. Virol.* **75,** 9633–9643
15. Bartelma, G., and Padmanabhan, R. (2002) Expression, purification, and characterization of the RNA 5′-triphosphatase activity of dengue virus type 2 nonstructural protein 3. *Virology* **299,** 122–132
16. Benarroch, D., Selisko, B., Locatelli, G. A., Maga, G., Romette, J. L., and Canard, B. (2004) The RNA helicase, nucleotide 5′-triphosphatase, and RNA 5′-triphosphatase activities of Dengue virus protein NS3 are Mg^{2+}-dependent and require a functional Walker B motif in the helicase catalytic core. *Virology* **328,** 208–218
17. Egloff, M. P., Benarroch, D., Selisko, B., Romette, J. L., and Canard, B. (2002) An RNA cap (nucleoside-2′-*O*)-methyltransferase in the flavivirus RNA polymerase NS5: crystal structure and functional characterization. *EMBO J.* **21,** 2757–2768
18. Egloff, M. P., Decroly, E., Malet, H., Selisko, B., Benarroch, D., Ferron, F., and Canard, B. (2007) Structural and functional analysis of methylation and 5′-RNA sequence requirements of short capped RNAs by the methyltransferase domain of dengue virus NS5. *J. Mol. Biol.* **372,** 723–736
19. Lu, G., and Gong, P. (2013) Crystal structure of the full-length Japanese encephalitis virus NS5 reveals a conserved methyltransferase-polymerase interface. *PLoS Pathog.* **9,** e1003549
20. Malet, H., Egloff, M. P., Selisko, B., Butcher, R. E., Wright, P. J., Roberts, M., Gruez, A., Sulzenbacher, G., Vonrhein, C., Bricogne, G., Mackenzie, J. M., Khromykh, A. A., Davidson, A. D., and Canard, B. (2007) Crystal structure of the RNA polymerase domain of the West Nile virus non-structural protein 5. *J. Biol. Chem.* **282,** 10678–10689
21. Ray, D., Shah, A., Tilgner, M., Guo, Y., Zhao, Y., Dong, H., Deas, T. S., Zhou, Y., Li, H., and Shi, P. Y. (2006) West Nile virus 5′-cap structure is formed by sequential guanine N-7 and ribose 2′-*O*-methylations by nonstructural protein 5. *J. Virol.* **80,** 8362–8370
22. Wu, J., Bera, A. K., Kuhn, R. J., and Smith, J. L. (2005) Structure of the flavivirus helicase: Implications for catalytic activity, protein interactions,

and proteolytic processing. *J. Virol.* **79,** 10268–10277
23. Bartholomeusz, A., and Thompson, P. (1999) Flaviviridae polymerase and RNA replication. *J. Viral Hepat.* **6,** 261–270
24. Nomaguchi, M., Ackermann, M., Yon, C., You, S., and Padmanabhan, R. (2003) De novo synthesis of negative-strand RNA by Dengue virus RNA-dependent RNA polymerase *in vitro*: nucleotide, primer, and template parameters. *J. Virol.* **77,** 8831–8842
25. Yap, T. L., Xu, T., Chen, Y. L., Malet, H., Egloff, M. P., Canard, B., Vasudevan, S. G., and Lescar, J. (2007) Crystal structure of the dengue virus RNA-dependent RNA polymerase catalytic domain at 1.85-angstrom resolution. *J. Virol.* **81,** 4753–4765
26. You, S., Falgout, B., Markoff, L., and Padmanabhan, R. (2001) *In vitro* RNA synthesis from exogenous dengue viral RNA templates requires long range interactions between 5′- and 3′-terminal regions that influence RNA structure. *J. Biol. Chem.* **276,** 15581–15591
27. Gualano, R. C., Pryor, M. J., Cauchi, M. R., Wright, P. J., and Davidson, A. D. (1998) Identification of a major determinant of mouse neurovirulence of dengue virus type 2 using stably cloned genomic-length cDNA. *J. Gen. Virol.* **79,** 437–446
28. Kapoor, M., Zhang, L., Ramachandra, M., Kusukawa, J., Ebner, K. E., and Padmanabhan, R. (1995) Association between NS3 and NS5 proteins of dengue virus type 2 in the putative RNA replicase is linked to differential phosphorylation of NS5. *J. Biol. Chem.* **270,** 19100–19106
29. Welsch, S., Miller, S., Romero-Brey, I., Merz, A., Bleck, C. K., Walther, P., Fuller, S. D., Antony, C., Krijnse-Locker, J., and Bartenschlager, R. (2009) Composition and three-dimensional architecture of the dengue virus replication and assembly sites. *Cell Host Microbe* **5,** 365–375
30. Mackenzie, J. M., and Westaway, E. G. (2001) Assembly and maturation of the flavivirus Kunjin virus appear to occur in the rough endoplasmic reticulum and along the secretory pathway, respectively. *J. Virol.* **75,** 10787–10799
31. Uchil, P. D., and Satchidanandam, V. (2003) Architecture of the flaviviral replication complex. Protease, nuclease, and detergents reveal encasement within double-layered membrane compartments. *J. Biol. Chem.* **278,** 24388–24398
32. Chen, C. J., Kuo, M. D., Chien, L. J., Hsu, S. L., Wang, Y. M., and Lin, J. H. (1997) RNA-protein interactions: Involvement of NS3, NS5, and 3′ noncoding regions of Japanese encephalitis virus genomic RNA. *J. Virol.* **71,** 3466–3473
33. Moreland, N. J., Tay, M. Y., Lim, E., Rathore, A. P., Lim, A. P., Hanson, B. J., and Vasudevan, S. G. (2012) Monoclonal antibodies against dengue NS2B and NS3 proteins for the study of protein interactions in the flaviviral replication complex. *J. Virol. Methods* **179,** 97–103
34. Yu, L., Takeda, K., and Markoff, L. (2013) Protein-protein interactions among West Nile non-structural proteins and transmembrane complex formation in mammalian cells. *Virology* **446,** 365–377
35. Johansson, M., Brooks, A. J., Jans, D. A., and Vasudevan, S. G. (2001) A small region of the dengue virus-encoded RNA-dependent RNA polymerase, NS5, confers interaction with both the nuclear transport receptor importin-ss and the viral helicase, NS3. *J. Gen. Virol.* **82,** 735–745
36. Brooks, A. J., Johansson, M., John, A. V., Xu, Y., Jans, D. A., and Vasudevan, S. G. (2002) The interdomain region of dengue NS5 protein that binds to the viral helicase NS3 contains independently functional importin beta 1 and importin α/β-recognized nuclear localization signals. *J. Biol. Chem.* **277,** 36399–36407
37. Zou, G., Chen, Y. L., Dong, H., Lim, C. C., Yap, L. J., Yau, Y. H., Shochat, S. G., Lescar, J., and Shi, P. Y. (2011) Functional analysis of two cavities in flavivirus NS5 polymerase. *J. Biol. Chem.* **286,** 14362–14372
38. Schreiber, M. J., Holmes, E. C., Ong, S. H., Soh, H. S., Liu, W., Tanner, L., Aw, P. P., Tan, H. C., Ng, L. C., Leo, Y. S., Low, J. G., Ong, A., Ooi, E. E., Vasudevan, S. G., and Hibberd, M. L. (2009) Genomic epidemiology of a dengue virus epidemic in urban Singapore. *J. Virol.* **83,** 4163–4173
39. Li, J., Lim, S. P., Beer, D., Patel, V., Wen, D., Tumanut, C., Tully, D. C., Williams, J. A., Jiricek, J., Priestle, J. P., Harris, J. L., and Vasudevan, S. G. (2005) Functional profiling of recombinant NS3 proteases from all four serotypes of dengue virus using tetrapeptide and octapeptide substrate libraries. *J. Biol. Chem.* **280,** 28766–28774
40. Paradkar, P. N., Ooi, E. E., Hanson, B. J., Gubler, D. J., and Vasudevan, S. G. (2011) Unfolded protein response (UPR) gene expression during antibody-dependent enhanced infection of cultured monocytes correlates with dengue disease severity. *Biosci. Rep.* **31,** 221–230
41. Dip, P. V., Kamariah, N., Manimekalai, M. S., Nartey, W., Balakrishna, A. M., Eisenhaber, F., Eisenhaber, B., and Grüber, G. (2014) The ups and downs in AhpF: structure, mechanism and ensemble formation of the alkylhydroperoxide reductase subunits AhpC and AhpF from *Escherichia coli*. *Acta Crystallogr. D Biol. Crystallogr.* **70,** 2848–2862
42. Svergun, D. (1993) A direct indirect method of small-angle scattering data treatment. *J. Appl. Crystallogr.* **26,** 258–267
43. Lipson, H. (1956) Small-angle scattering of x-rays by Guinier, A., and Fournet, G. *Acta Crystallogr.* **9,** 839
44. Svergun, D. (1992) Determination of the regularization parameter in indirect-transform methods using perceptual criteria. *J. Appl. Crystallogr.* **25,** 495–503
45. Svergun, D. I., Petoukhov, M. V., and Koch, M. H. (2001) Determination of domain structure of proteins from x-ray solution scattering. *Biophys. J.* **80,** 2946–2953
46. Kozin, M. B., and Svergun, D. I. (2002) Automated matching of high- and low-resolution structural models. *J. Appl. Crystallogr.* **34,** 33–41
47. Bernadó, P., Mylonas, E., Petoukhov, M. V., Blackledge, M., and Svergun, D. I. (2007) Structural characterization of flexible proteins using small-angle x-ray scattering. *J. Am. Chem. Soc.* **129,** 5656–5664
48. Petoukhov, M. V., Franke, D., Shkumatov, A. V., Tria, G., Kikhney, A. G., Gajda, M., Gorba, C., Mertens, H. D., Konarev, P. V., and Svergun, D. I. (2012) New developments in the ATSAS program package for small-angle scattering data analysis. *J. Appl. Crystallogr.* **45,** 342–350
49. Wang, R. F., and Kushner, S. R. (1991) Construction of versatile low-copy-number vectors for cloning, sequencing and gene expression in *Escherichia coli*. *Gene* **100,** 195–199
50. Johnson, B. W., Russell, B. J., and Lanciotti, R. S. (2005) Serotype-specific detection of dengue viruses in a fourplex real time reverse transcriptase PCR assay. *J. Clin. Microbiol.* **43,** 4977–4983
51. Plaskon, N. E., Adelman, Z. N., and Myles, K. M. (2009) Accurate strand-specific quantification of viral RNA. *PLoS One* **4,** e7468
52. Collins, T. J. (2007) ImageJ for microscopy. *BioTechniques* **43,** 25–30
53. Moreland, N. J., Tay, M. Y., Lim, E., Paradkar, P. N., Doan, D. N., Yau, Y. H., Geifman Shochat, S., and Vasudevan, S. G. (2010) High affinity human antibody fragments to dengue virus non-structural protein 3. *PLoS Negl. Trop. Dis.* **4,** e881
54. Rivino, L., Kumaran, E. A., Jovanovic, V., Nadua, K., Teo, E. W., Pang, S. W., Teo, G. H., Gan, V. C., Lye, D. C., Leo, Y. S., Hanson, B. J., Smith, K. G., Bertoletti, A., Kemeny, D. M., and MacAry, P. A. (2013) Differential targeting of viral components by $CD4^+$ *versus* $CD8^+$ T lymphocytes in dengue virus infection. *J. Virol.* **87,** 2693–2706
55. Takahashi, H., Takahashi, C., Moreland, N. J., Chang, Y. T., Sawasaki, T., Ryo, A., Vasudevan, S. G., Suzuki, Y., and Yamamoto, N. (2012) Establishment of a robust dengue virus NS3-NS5 binding assay for identification of protein-protein interaction inhibitors. *Antiviral Res.* **96,** 305–314
56. Derossi, D., Calvet, S., Trembleau, A., Brunissen, A., Chassaing, G., and Prochiantz, A. (1996) Cell internalization of the third helix of the Antennapedia homeodomain is receptor-independent. *J. Biol. Chem.* **271,** 18188–18193
57. Keller, A. A., Mussbach, F., Breitling, R., Hemmerich, P., Schaefer, B., Lorkowski, S., and Reissmann, S. (2013) Relationships between cargo, cell penetrating peptides and cell type for uptake of non-covalent complexes into live cells. *Pharmaceuticals* **6,** 184–203
58. Zorko, M., and Langel, U. (2005) Cell-penetrating peptides: mechanism and kinetics of cargo delivery. *Adv. Drug Deliv. Rev.* **57,** 529–545
59. Luo, D., Wei, N., Doan, D. N., Paradkar, P. N., Chong, Y., Davidson, A. D., Kotaka, M., Lescar, J., and Vasudevan, S. G. (2010) Flexibility between the protease and helicase domains of the dengue virus NS3 protein conferred by the linker region and its functional implications. *J. Biol. Chem.* **285,** 18817–18827
60. Svergun, D. I., Koch, M. H., Timmins, P. A., and May, R. P. (2013) *Small Angle X-Ray and Neutron Scattering from Solutions of Biological Macromolecules*, Oxford University Press, Oxford, UK
61. Grüber, A., Gunalan, K., Ramalingam, J. K., Manimekalai, M. S., Grüber,

G., and Preiser, P. R. (2011) Structural characterization of the erythrocyte binding domain of the reticulocyte binding protein homologue family of *Plasmodium yoelii*. *Infect. Immun.* **79,** 2880–2888
62. Ho, C. S., Rydstrom, A., Manimekalai, M. S., Svanborg, C., and Grüber, G. (2012) Low resolution solution structure of HAMLET and the importance of its α-domains in tumoricidal activity. *PLoS ONE* **7,** e53051
63. Balakrishna, A. M., Manimekalai, M. S., Hunke, C., Gayen, S., Rössle, M., Jeyakanthan, J., and Grüber, G. (2010) Crystal and solution structure of the C-terminal part of the *Methanocaldococcus jannaschii* A1AO ATP synthase subunit E revealed by X-ray diffraction and small-angle X-ray scattering. *J. Bioenerg. Biomembr.* **42,** 311–320
64. Svergun, D. I., Konrad, S., Huss, M., Koch, M. H., Wieczorek, H., Altendorf, K., Volkov, V. V., and Grüber, G. (1998) Quaternary structure of V1 and F1 ATPase: significance of structural homologies and diversities. *Biochemistry* **37,** 17659–17663
65. Davidson, A. D. (2014) Development and application of dengue virus reverse genetic systems. *Methods Mol. Biol.* **1138,** 113–130
66. Tomassini, J. E., Boots, E., Gan, L., Graham, P., Munshi, V., Wolanski, B., Fay, J. F., Getty, K., and LaFemina, R. (2003) An *in vitro* Flaviviridae replicase system capable of authentic RNA replication. *Virology* **313,** 274–285
67. Chu, P. W., and Westaway, E. G. (1985) Replication strategy of Kunjin virus: evidence for recycling role of replicative form RNA as template in semiconservative and asymmetric replication. *Virology* **140,** 68–79
68. Lescar, J., Luo, D., Xu, T., Sampath, A., Lim, S. P., Canard, B., and Vasudevan, S. G. (2008) Towards the design of antiviral inhibitors against flaviviruses: the case for the multifunctional NS3 protein from Dengue virus as a target. *Antiviral Res.* **80,** 94–101
69. Rawlinson, S. M., Pryor, M. J., Wright, P. J., and Jans, D. A. (2006) Dengue virus RNA polymerase NS5: a potential therapeutic target? *Curr. Drug Targets* **7,** 1623–1638
70. Bollati, M., Alvarez, K., Assenberg, R., Baronti, C., Canard, B., Cook, S., Coutard, B., Decroly, E., de Lamballerie, X., Gould, E. A., Grard, G., Grimes, J. M., Hilgenfeld, R., Jansson, A. M., Malet, H., Mancini, E. J., Mastrangelo, E., Mattevi, A., Milani, M., Moureau, G., Neyts, J., Owens, R. J., Ren, J., Selisko, B., Speroni, S., Steuber, H., Stuart, D. I., Unge, T., and Bolognesi, M. (2010) Structure and functionality in flavivirus NS-proteins: perspectives for drug design. *Antiviral Res.* **87,** 125–148
71. Geiss, B. J., Stahla, H., Hannah, A. M., Gari, A. M., and Keenan, S. M. (2009) Focus on flaviviruses: current and future drug targets. *Future Med. Chem.* **1,** 327–344
72. Li, X. D., Shan, C., Deng, C. L., Ye, H. Q., Shi, P. Y., Yuan, Z. M., Gong, P., and Zhang, B. (2014) The interface between methyltransferase and polymerase of NS5 is essential for flavivirus replication. *PLoS Negl. Trop. Dis.* **8,** e2891
73. Brugidou, J., Legrand, C., Méry, J., and Rabié, A. (1995) The retro-inverso form of a homeobox-derived short peptide is rapidly internalised by cultured neurones: a new basis for an efficient intracellular delivery system. *Biochem. Biophys. Res. Commun.* **214,** 685–693
74. Thompson, J. D., Higgins, D. G., and Gibson, T. J. (1994) CLUSTAL W: improving the sensitivity of progressive multiple sequence alignment through sequence weighting, position-specific gap penalties and weight matrix choice. *Nucleic Acids Res.* **22,** 4673–4680